"Two-step" electron transfer and mechanisms of electrochemically induced reactions of the MeCCo3(CO)9 cluster and its phosphine derivatives

ARTICLE *in* JOURNAL OF THE AMERICAN CHEMICAL SOCIETY · JULY 1989

Impact Factor: 12.11 · DOI: 10.1021/ja00196a010

"Two-Step" Electron Transfer and Mechanisms of Electrochemically Induced Reactions of the $MeCCo_3(CO)_9$ Cluster and Its Phosphine Derivatives

Klaus Hinkelmann,[1a] Jürgen Heinze,*[1a] Hans-Thomas Schacht,[1b] John S. Field,[1b,c] and Heinrich Vahrenkamp*[1b]

Contribution from the Institut für Physikalische Chemie and the Institut für Anorganische Chemie, Universität Freiburg, Albertstrasse 21, D-7800 Freiburg, Federal Republic of Germany.
Received December 5, 1988

Abstract: The electrochemistry of the methylidyne tricobalt nonacarbonyl cluster and of its phosphine-substituted derivatives has been reinvestigated. For this purpose six missing members of the series were prepared. The compounds $MeCCo_3(CO)_{9-n}L_n$ for L = PMe_3, n = 1-3; L = PMe_2Ph, n = 1-3; L = $PMePh_2$, n = 1, 2; L = PPh_3, n = 1; L = PEt_2Ph, n = 3, were studied by cyclic voltammetry. By varying the ligands, the electrodes, the sweep ranges and rates, the temperatures, the concentrations, and the solvents and by running the experiments in the presence of excess ligands, a consistent set of data was obtained. In contrast to widespread opinion, the radical anion (49-electron complex) of the parent cluster $MeCCo_3(CO)_9$ is of limited stability due to the reversible elimination of CO. Analogously, the 49-electron anions of the phosphine-substituted clusters can eliminate one phosphine ligand producing 47-electron monoanions $[MeCCo_3(CO)_{9-n}L_{n-1}]^-$. Further reduction of these 47-electron monoanions to their 48-electron dianions occurs more easily than that of the starting clusters $MeCCo_3(CO)_{9-n}L_n$ (ECE mechanism). Depending on the kind and number of phosphine ligands, $[MeCCo_3(CO)_{9-n}L_n]^-$ can alternatively eliminate CO. The ligand-deficient 47-electron species are the key intermediates in the electron-transfer-induced dissociative ligand substitutions; as such they are capable of either reacting with liberated phosphine or CO or alternatively of being reduced to the dianions. Elimination of CO followed by addition of phosphine occurs over an ETC ligand substitution path. On the reverse electrochemical sweep, the ligand-deficient 48-electron dianions can be reoxidized to the 47-electron monoanions. In some cases further oxidation to the ligand-deficient neutral 46-electron species $MeCCo_3(CO)_{9-n}L_{n-1}$ occurs, which are converted back to the starting cluster complexes by ligand addition (EEC mechanism). The proposed reaction path including a homogeneous disproportionation is supported by a crossover phenomenon observed in the cyclic voltammograms of the trisphosphine-substituted clusters. Probably for steric reasons both the stability of the 49-electron cluster radical anions and the extent of ETC ligand substitution vs two-electron reduction increase with the number of methyl groups on the PR_3 ligands, i.e., PMe_3 > ... > PPh_3; moreover, they decrease with the number of PR_3 ligands. The opposite holds true for the stability of the 47-electron intermediates. Their remarkable stability in the case of $MeCCo_3(CO)_6L_3$ has allowed an investigation of their reactions with CO and phosphines from which the dissociative mechanism of the electron-transfer-induced ligand substitutions in the $RCCo_3$ clusters could be additionally confirmed. The cyclic voltammograms including the crossover phenomenon can be simulated by using the above-mentioned electrochemical steps and a ligand-dependent set of kinetic parameters. In addition to the well-established ETC-catalyzed substitution of CO by phosphine ligands, the measurements have shown that in the presence of CO the phosphine ligands can be replaced successively in an "inverse" ETC-catalyzed reaction.

The electrochemistry and redox chemistry of metal-metal bonded organometallic species, originally used to evaluate bond strengths[2] and electron distributions,[3] has been refined to a point where group trends can be discussed,[4,5] applications to organic synthesis begin to emerge,[6] and intricate details, e.g., of the changes in complex geometries due to electron transfer[7] or the mechanisms of electron-transfer-catalyzed ligand substitutions,[8-11] become accessible. Due to the improvements in instrumentation and interpretation[12,13] it has turned out that some of the original results deserve reevaluation and some of the well-investigated systems can be brought to a better understanding. A typical example for this are the possible existence and fate of the organometallic radicals generated by Mn-Mn bond cleavage in $Mn_2(CO)_{10}$ or by oxidation of $Mn(CO)_5^-$ and of similar species derived from substituted manganese and rhenium carbonyls.[14] One of the frequently investigated metal-metal bonded compounds is the

(1) (a) Institut für Physikalische Chemie. (b) Institut für Anorganische Chemie. (c) On leave of absence from the University of Natal, Pietermaritzburg, South Africa.
(2) Dessy, R. E.; Bares, L. *Acc. Chem. Res.* **1972**, *5*, 415-421.
(3) Meyer, T. J. *Prog. Inorg. Chem.* **1975**, *19*, 1-50.
(4) (a) Lemoine, P. *Coord. Chem. Rev.* **1982**, *47*, 55-88. (b) Lemoine, P. *Coord. Chem. Rev.* **1988**, *83*, 169-197.
(5) Geiger, W. E.; Conelly, N. G. *Adv. Organomet. Chem.* **1985**, *24*, 87-130.
(6) Freeman, M. J.; Orpen, A. G.; Conelly, N. G.; Manners, I. I.; Raven, S. J. *J. Chem. Soc., Dalton Trans.* **1985**, 2283-2289. Conelly, N. G.; Farrow, N. J.; Knox, S. A. R.; MacPherson, K. A.; Orpen, A. G. *J. Chem. Soc., Chem. Commun.* **1985**, 16-17.
(7) Geiger, W. E. *Prog. Inorg. Chem.* **1985**, *33*, 275-352. (b) Moulton, R. D.; Chandler, D. J.; Arif, A. M.; Jones, R. A.; Bard, A. J. *J. Am. Chem. Soc.* **1988**, *110*, 5714-5725. (c) Moulton, R.; Weidman, T. W.; Vollhardt, K. P. C.; Bard, A. J. *Inorg. Chem.* **1986**, *25*, 1846-1851.
(8) Bezems, G. J.; Rieger, P. H.; Visco, S. *J. Chem. Soc., Chem. Commun.* **1981**, 265-266.
(9) (a) Hershberger, J. W.; Kochi, J. K. *J. Chem. Soc., Chem. Commun.* **1982**, 212-214. (b) Hershberger, J. W.; Klinger, R. J.; Kochi, J. K. *J. Am. Chem. Soc.* **1983**, *105*, 61-73. (c) Ohst, H. H; Kochi, J. K. *Inorg. Chem.* **1986**, *25*, 2066-2074. (d) Richmond, M. G.; Kochi, J. K. *Inorg. Chem.* **1986**, *25*, 656-665. (e) Ohst, H. H.; Kochi, J. K. *J. Am. Chem. Soc.* **1986**, *108*, 2897-2908.
(10) (a) Arewgoda, C. M.; Robinson, B. H.; Simpson, J. J. *J. Chem. Soc., Chem. Commun.* **1982**, 284-285. (b) Arewgoda, M.; Rieger, P. H.; Robinson, B. H.; Simpson, J.; Visco, S. J. *J. Am. Chem. Soc.* **1982**, *104*, 5633-5640. (c) Arewgoda, M.; Robinson, B. H.; Simpson, J. *J. Am. Chem. Soc.* **1983**, *105*, 1893-1903. (d) Cunningham, R. G.; Downard, A. J.; Hanton, L. R.; Jensen, S. D.; Robinson, B. H.; Simpson, J. *Organometallics* **1984**, *3*, 180-182. (e) Cunningham, R. G.; Hanton, L. R.; Jensen, S. D.; Robinson, B. H.; Simpson, J. *Organometallics* **1987**, *6*, 1470-1479. (f) Jensen, S. D.; Robinson, B. H.; Simpson, J. *Organometallics* **1987**, *6*, 1479-1485.
(11) (a) Darchen, A.; Mahe, C.; Patin, H. *J. Chem. Soc., Chem. Commun.* **1982**, 243-245. (b) Darchen, A.; Mahe, C.; Patin, H. *Nouv. J. Chim.* **1982**, *6*, 539-546. (c) Lhadi El Kbir, Mahe, C.; Patin, H.; Darchen, A. *J. Organomet. Chem.* **1983**, *246*, C61-C64. (d) Darchen, A.; Lhadi El Kbir; Patin, H. *J. Organomet. Chem.* **1983**, *259*, 189-206.
(12) Heinze, J. *Angew. Chem.* **1984**, *96*, 823-840; *Angew. Chem., Int. Ed. Engl.* **1984**, *23*, 831-847.
(13) Zizelman, P. M.; Amatore, C.; Kochi, J. K. *J. Am. Chem. Soc.* **1984**, *106*, 3771-3784.
(14) Walker, H. W.; Rattinger, G. B.; Belford, R. L.; Brown, T. L. *Organometallics* **1983**, *2*, 775-776, and references therein. Lemoine, P.; Giraudeau, A.; Gross, M.; Braunstein, P. *J. Organomet. Chem.* **1980**, *202*, 455-468.

0002-7863/89/1511-5078$01.50/0

tricobalt carbon cluster, $RCCo_3(CO)_9$,[15] where alterations were introduced by means of ligand substitution,[16] by metal substitution,[17] and then by a complete variation of metal and capping units in the EM_3 tetrahedron.[18] In each case the electrochemistry became more complicated due to seemingly nonintegral numbers of transferred electrons and/or rapid decomposition and/or electron-induced subsequent reactions.

We were attracted to reinvestigate this situation by the possible occurrence of two-electron transfers in the $RCCo_3(CO)_{9-n}L_n$[16a-c] as well as in the $RCCo_2MCp(CO)_8$[18] systems. Since the compounds $RCCo_3(CO)_{9-n}L_n$ (n = 1–3) are easily accessible, they offered a chance for a better understanding of two-electron redox reactions which, for polynuclear complexes, so far have been associated mainly with making and breaking of metal–metal bonds.[7] However, the general importance of two-electron redox reactions for practical chemistry, e.g., in the SO_2/SO_3 or alcohol/ketone interconversions and the possible use of polymetallic compounds to catalyze such interconversions, offer many reasons to study two-electron transfers in general.

It is well accepted that "two-electron" redox processes proceed in at least two steps, each of which has its own activation barrier.[19,20] From a mechanistic point of view, they fall into two categories. In the EE-type mechanism, one of the charge-transfer steps is concurrent with a structural change (in the substrate or the solvation shell). In the case of the ECE-type mechanism an intervening chemical step takes place (including isomerization, changes in the ligand sphere, or other subsequent reactions). Up to now cyclic voltammetry[12] was one of the preferred methods for the analysis of the EE mechanism[21] as well as for the ECE mechanism.[7b,c,22] It has also revealed that the foregoing schemes must be refined by introducing additional reaction paths for the reverse reaction.[7,21,22] In the literature, EE mechanisms as well as ECE mechanisms have been proposed as reduction paths for tricobalt carbon clusters.[16c,d]

To get a more complete picture of the redox chemistry of substituted derivatives of the tricobalt carbon cluster, we synthesized the missing compounds in the series $MeCCo_3(CO)_{9-n}L_n$, which is now complete for L = PMe_3, n = 1–3; L = PMe_2Ph, n = 1–3; L = $PMePh_2$, n = 1, 2; and L = PPh_3, n = 1. The clusters were subjected to comprehensive voltammetric measurements by varying the electrodes, the sweep conditions, the temperatures, the solvents, and the coligands. This has allowed us to develop an interpretation of the redox behavior that is consistent with all observations.

When this work was close to completion, several papers by Robinson et al. appeared reporting related investigations on $RCCo_3(CO)_9$ (R = Me, Ph) derivatives with one PPh_3 or one bidentate ligand.[16c-e] Of these, $MeCCo_3(CO)_8PPh_3$ seemed to undergo a reversible two-electron reduction.[16c] This was, however, inconsistent with the proposed ECE mechanism, where the chemical step was presumed to be a reversible phosphine elimination. The reported experimental work was not able to clarify this inconsistency.

Scheme I

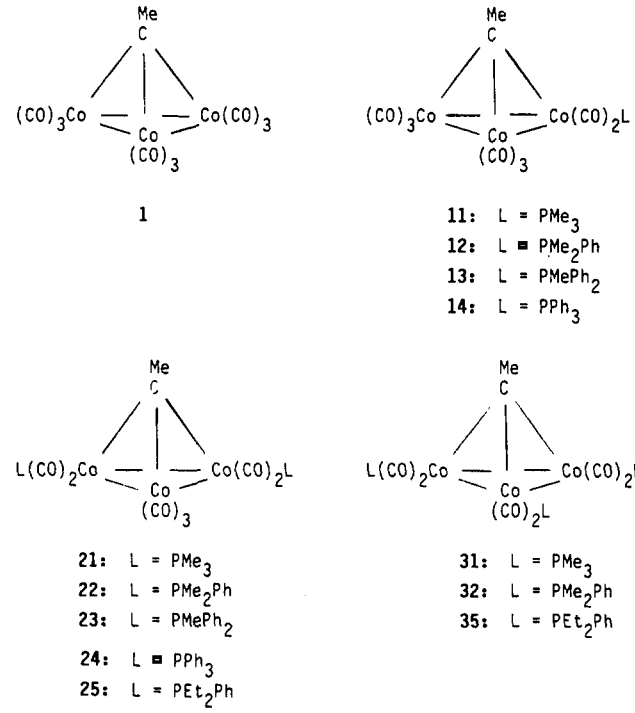

In a recent communication[23] we reported preliminary results on the reduction of $MeCCo_3(CO)_6L_3$ (L = PMe_2Ph, PEt_2Ph) that have unequivocally identified phosphine elimination as the first successive step following radical anion formation. The resulting ligand-deficient 47e species were further reduced to the corresponding dianions, which could be reoxidized in two steps. The 47e species were remarkably stable.

In the present study we have identified phosphine elimination as the main reaction path during the reduction of the complete series of phosphine-substituted $RCCo_3$ clusters. Moreover, in the case of mono- and disubstituted clusters cyclic voltammetry has revealed a complicated reaction behavior. We could show that this is due to the intermediate stability of their radical anions and the competition between elimination of CO and phosphine ligands. The occurrence of crossover effects,[24] isopotential points,[25] and the ETC pattern[26] in some of the obtained cyclic voltammograms was a valuable aid in resolving the puzzling variety of experimental results. In contrast to widespread opinion we also found that the $MeCCo_3(CO)_9$ cluster is not stable upon reduction but decomposes by a slow CO elimination.

The compounds under investigation are listed in Scheme I. To improve the readability of the text a two-digit numbering scheme is used for the phosphine-substituted clusters. The first digit indicates the degree of substitution (**1–3**), the second digit indicates the phosphine ligand as shown in the scheme. The letter **a** attached to the number indicates the compound with one missing CO ligand.

(15) (a) Kotz, J. C.; Petersen, Reed, R. C. *J. Organomet. Chem.* **1976**, *120*, 433–437. (b) Bond, A. M.; Peake, B. M.; Robinson, B. H.; Simpson, J.; Watson, D. J. *Inorg. Chem.* **1977**, *16*, 410–415. (c) Peake, B. M.; Rieger, P. H.; Robinson, B. H.; Simpson, J. *Inorg. Chem.* **1979**, *18*, 1000–1005. (d) Colbran, S. B.; Robinson, B. H.; Simpson, J. *Organometallics* **1983**, *2*, 943–951.

(16) (a) Bond, A. M.; Dawson, P. A.; Peake, B. M.; Rieger, P. H.; Robinson, B. H.; Simpson, J. *Inorg. Chem.* **1979**, *18*, 1413–1417. (b) Colbran, S. B.; Robinson, B. H.; Simpson, J. *Organometallics* **1983**, *2*, 952–957. (c) Downard, A. J.; Robinson, B. H.; Simpson, J. *Organometallics* **1986**, *5*, 1122–1131. (d) Downard, A. J.; Robinson, B. H.; Simpson, J. *Organometallics* **1986**, *5*, 1132–1140. (e) Downard, A. J.; Robinson, B. H.; Simpson, J. *Organometallics* **1986**, *5*, 1140–1149.

(17) (a) Beurich, H.; Vahrenkamp, H. *Chem. Ber.* **1982**, *115*, 2385–2408. (b) Beurich, H.; Blumhofer, R.; Vahrenkamp, H. *Chem. Ber.* **1982**, *115*, 2409–2422.

(18) Lindsay, P. N.; Peake, B. M.; Robinson, B. H.; Simpson, J.; Honrath, U.; Vahrenkamp, H.; Bond, A. M. *Organometallics* **1984**, *3*, 413–426.

(19) Conway, B. E.; Bockris, J. O'M. *Electrochim. Acta* **1961**, *3*, 340–366.

(20) Vetter, K. J. *Elektrochemische Kinetik*; Springer: Berlin, 1961; *Electrochemical Kinetics*; Academic Press: New York, 1947.

(21) Hinkelmann, K.; Heinze, J. *Ber. Bunsen-Ges. Phys. Chem.* **1987**, *91*, 243–249, and references therein.

(22) Dietrich, M.; Heinze, J.; Fischer, H.; Neugebauer, F. A. *Angew. Chem.* **1986**, *98*, 999–1000; *Angew. Chem., Int. Ed. Engl.* **1986**, *25*, 1021–1023.

(23) Hinkelmann, K.; Mahlendorf, F.; Heinze, J.; Schacht, H. T.; Field, J. S.; Vahrenkamp, H. *Angew. Chem.* **1987**, *99*, 373–374; *Angew. Chem., Int. Ed. Engl.* **1987**, *26*, 352–354.

(24) (a) Pinson, J.; Saveant, J. M. *J. Am. Chem. Soc.* **1978**, *100*, 1506–1510. (b) Amatore, C.; Chaussard, J.; Pinson, J.; Saveant, J. M.; Thiebault, A. *J. Am. Chem. Soc.* **1979**, *101*, 6012–6020. (c) Amatore, C.; Pinson, J.; Saveant, J. M.; Thiebault, A. *J. Electroanal. Chem.* **1980**, *107*, 59–74.

(25) (a) Untereker, D. F.; Bruckenstein, S. *Anal. Chem.* **1972**, *44*, 1009–1020. (b) Untereker, D. F.; Bruckenstein, S. *J. Electroanal. Chem.* **1974**, *57*, 77–87. (c) Day, R. W.; Inzelt, G.; Kinstle, J. L.; Chambers, J. Q. *J. Am. Chem. Soc.* **1982**, *104*, 6804–6805.

(26) (a) Saveant, J. M. *Acc. Chem. Res.* **1980**, *13*, 323–329. (b) Chanon, M. *Acc. Chem. Res.* **1987**, *20*, 214–221. (c) Astruc, D. *Angew. Chem.* **1988**, *100*, 662–680; *Angew. Chem., Int. Ed. Engl.* **1988**, *27*, 643–660.

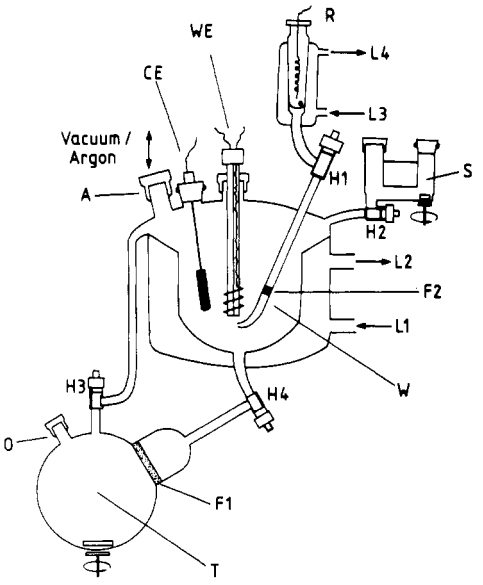

Figure 1. Electrochemical cell for electroanalytical measurements under superdry conditions. W: undivided cell compartment for combined working/counter electrode (WE), or working electrode (WE) and counter electrode (CE). R: reference electrode compartment. A: connection to vacuum/inert gas facilities. O: NS-14 standard joint with rubber septum. T: storage vessel for superactive alumina and solvent–electrolyte system. S: storage compartment for electroactive species. F1, F2: glas frit of porosity 3. H1–H4: high vacuum O-ring taps. L1–L4: connections to cooling jacket.

Thereby all observed compounds, even those missing PR_3 ligands, can be numbered, since a cluster missing CO is identical with a cluster of the more highly substituted series missing PR_3, i.e., **21** − CO = **31** − PR_3 = **21a**, etc.

Experimental Section

Preparative Procedures. All preparations were done under an atmosphere of purified nitrogen in solvents distilled under nitrogen. IR spectra were recorded on a Perkin-Elmer 782 instrument, NMR spectra on a Varian EM 360 A machine. The known compounds **11**,[27] **14**,[28] **21**,[27] and **35**[28] were prepared according to published procedures. All preparative details and the elemental analyses of the new compounds are given in the supplementary material (see paragraph at the end of the paper).

The new clusters were prepared as follows: The starting cluster **1** was dissolved in hexane. The ligand was added as a 0.1 M hexane solution. The mixture was stirred for the given time at the given temperature and then evacuated to dryness in vacuo. The residue was chromatographed with benzene/hexane (1:4) over a 60 × 3.5 cm silica gel column. The fractions used for cyclic voltammetry and elemental analysis were recrystallized twice from *n*-hexane at −30 °C.

Electrochemical Measurements. Our standard electrochemical instrumentation consisted of a PAR potentiostat/galvanostat Model 173 and a PAR universal programmer Model 175. Cyclic voltammograms with scan rates up to 1 V s^{-1} were recorded with a Model 2000 Bryant *X–Y* recorder. For scan rates higher than 1 V s^{-1} a model TM 509 Maurer transient recorder was used. A three-electrode configuration was employed throughout. The working electrodes were either Pt disks (diameter 0.81 and 1.39 mm, respectively), sealed in soft glass, or commercial Metrohm EA290 HMDEs. The counter electrode was a Pt wire coiled around the glass mantle of the working electrode or a separate Pt foil. The reference electrode was an Ag wire, on which AgCl had been deposited electrolytically, immersed in the electrolyte solution. Potentials were calibrated against the formal potential of the Fc/Fc^+ couple (+0.352 V vs Ag/AgCl). All manipulations were carried out under an argon atmosphere.

The experiments were performed in specially designed cells allowing complete exclusion of oxygen and moisture that are described here for the first time. Their prominent feature is the possibility of internally drying the solvent/electrolyte system[29] and storing the substrate in an adjacent compartment from which it can be rinsed into the working electrode compartment with the aid of the solvent. Thus, inert gas conditions were secured throughout the measurements. Figure 1 shows a schematic sketch of a typical cell. The cell was connected to the vacuum/inert gas facilities by means of a flexible metal tube closed at A with a rubber septum. Cooling mantles are fused around the working electrode compartment W (connections L_1, L_2) and the reference electrode compartment R (connections L_3, L_4), respectively. The working electrode compartment is connected via the plugs H3 and H4 with vessel T which is filled with desiccant (typically basic Al_2O_3, Woelm). The configuration of the electrodes was chosen to warrant minimal distances.

Sample preparations started with heating the cell, desiccant, and supporting electrolyte under vacuum conditions (H1–H3 opened; H4 closed). Then H1–H3 were closed, and the working electrode compartment W was filled with argon. The solvent was then transferred by a syringe from a stock vessel to the cell via A. After complete dissolution of the supporting electrolyte, the solvent system was cooled to −30 °C. Stopcock H4 was then opened, and the solution transfered to the evacuated desiccant vessel T. The suspension was stirred by a magnetic bar, and the cell then lifted clockwise by ca. 80°. Care was taken that the suspended Al_2O_3 covered the frit F1 before the solvent system was transferred back to W. After the working electrode compartment had been refilled, the evacuated reference electrode compartment R was filled by opening H1. After checking voltammetrically the purity of the solvent system, the substrate could be introduced under inert gas conditions in a straightforward manner.

Alternatively, the more time-consuming drying procedure of condensing the solvent onto the desiccant could be applied, thus allowing measurements of substrates that were exceedingly moisture sensitive.

The solvents used were purified by published methods: CH_2Cl_2[30] and CH_3CN.[31] All clusters were subjected to cyclic voltammetry in CH_3CN/0.1 M $TBAPF_6$ at temperatures between −43 and +24 °C, using scan rates between 0.01 and 150 V s^{-1}. Additional measurements were conducted in CH_2Cl_2 (0.1 M $TBABF_4$ or 0.1 M $TBAClO_4$).

The solutions of the mono- and disubstituted cluster derivatives gave no indication of decomposition when stored at room temperature for several days, as revealed by repeated cyclic voltammograms. In the case of the trisubstituted derivatives, however, cyclic voltammograms showed the appearance of minor amounts of decomposition products after 3 days.

Digital Simulations. Digital simulations were performed by using the implicit Crank–Nicholson technique.[32a] All boundary conditions were formulated implicitly.[32b] It was assumed that the disproportionation reaction is in a dynamic equilibrium.

Results and Discussion

New Compounds. Although quite a number of ligand-substituted derivatives of the tricobalt carbon cluster are known,[27,28] six of the twelve phosphine derivatives listed in Scheme I were unknown, one (**24**) was known to be unstable,[16d] and one (**25**) is observed only as an intermediate here. It was, however, no problem to prepare the six unknown ones by thermal phosphine substitutions, with the rate of CO substitution increasing with the number of methyl groups in the phosphine, i.e., fastest for PMe_3. The degree of substitution varied systematically with the type of ligand: trisubstituted derivatives were accessible with PMe_3 and PMe_2Ph, disubstituted derivatives with $PMePh_2$, and only the monosubstituted derivative with PPh_3. Thus the steric bulk of the ligands controls the reactions and limits systematically the accessibility of substituted derivatives by thermal methods. It was impossible to direct the substitutions to just one derivative. Accordingly, the product mixtures always had to be separated by column chromatography.

The new clusters were easily identified by their spectra; cf. tables in the supplementary material. There is a systematic shift in the C–Me and P–Me NMR resonances with increasing substitution. The IR spectra show absorptions for bridging CO groups for the di- and trisubstituted clusters, a phenomenon that can also be attributed to the steric bulk of the ligands. The simplest deter-

(27) Beurich, H.; Vahrenkamp, H. *Chem. Ber.* **1981**, *114*, 2542–2567.
(28) Matheson, T. W.; Robinson, B. H.; Tham, W. S. *J. Chem. Soc. A* **1971**, 1457–1463.
(29) (a) Lines, R.; Svensmark, V.; Parker, V. D. *Acta Chem. Scand.* **1978**, *B32*, 510–514. (b) Kiesele, H. *Anal. Chem.* **1981**, *53*, 1952–1954.
(30) Bekkevoll, S.; Svorstol, I.; Hoiland, H.; Songstad J. *Acta Chem. Scand.* **1983**, *B37*, 935.
(31) Coetzee, J. F. *Recommended Methods for Purification of Solvents*; Pergamon: Oxford 1982.
(32) (a) Heinze, J.; Störzbach, M.; Mortensen, J. *J. Electroanal. Chem.* **1984**, *165*, 61–70. (b) Britz, D.; Heinze, J.; Störzbach, M.; Mortensen, J. *J. Electroanal. Chem.* **1988**, *240*, 27–43.

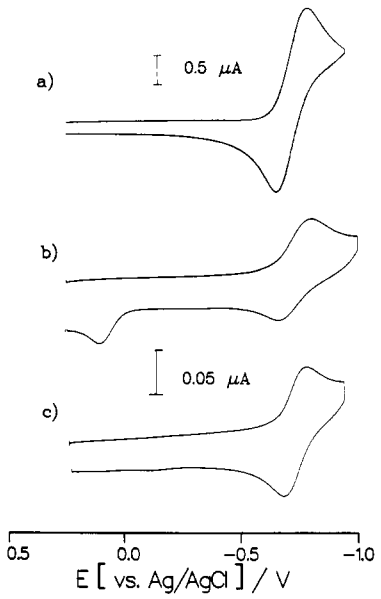

Figure 2. Cyclic voltammograms of **1** in dry acetonitrile with 0.1 M $TBAPF_6$ as supporting electrolyte; scan rate 0.2 V s^{-1}; T = 24 °C. (a) 2.4×10^{-3} M; (b) 7.2×10^{-5} M; (c) 7.2×10^{-5} M after addition of CO.

mination of the degree of substitution is by the color of the compounds: brown for n = 1, red–brown for n = 2, and deep red for n = 3.

Electrochemical Studies of μ_3-$MeCCo_3(CO)_9$ (1). The electrochemical reduction of unsubstituted tricobalt carbonyl clusters such as **1** is well known in the literature.[15] From cyclic voltammetry and ESR results, it was concluded that **1** forms a stable monoanion ($E_{1/2}$ = −0.745 V vs Ag/AgCl), which may be used as a one-electron standard. Further reduction of $[\mathbf{1}]^-$ to $[\mathbf{1}]^{2-}$ at E_{pc} = −2.23 V was reported to be chemically irreversible, leading to the formation of $[Co(CO)_4]^-$, whose oxidation is observed voltammetrically at E_{pa} = 0.07 V.[15]

At first sight, our voltammetric measurements carried out with standard concentrations of **1** ($c = 1 \times 10^{-3}$ M) seemed to confirm these results. Cyclic voltammograms of the first reduction step obtained in superdry CH_3CN at a Pt disk electrode clearly correspond to a reversible redox step (Figure 2a). However, when the concentration is lowered below 10^{-4} M, cyclic voltammetry exhibits waves with a current ratio i_{pa}/i_{pc} of less than 0.8, indicating a chemical follow-up reaction. In addition, in the reverse scan at E_{pa} = 0.07 V a new anodic wave is observed (Figure 2b). In agreement with the data of the dianion decomposition[15b] this can be attributed to the oxidation of the decomposition product $[Co(CO)_4]^-$. In the presence of CO the oxidation wave for $[Co(CO)_4]^-$ disappears and the cyclic voltammetric response for the reduction of **1** again becomes fully reversible (Figure 2c). The same effect is observed when the concentration of **1** is increased to 10^{-3} M or when high scan rates are used.

These results clearly indicate that after the formation of the 49e radical anion $[\mathbf{1}]^-$ a chemical reaction takes place during which a CO ligand is eliminated from the cluster resulting in the 47e species $[MeCCo_3(CO)_8]^-$ (**1a**). The fact that the decomposition reaction, which is slow on the time scale of the voltammetric experiment, is noticeable only at low concentrations of **1** proves that the CO elimination is a reversible process. While the elimination of CO from **1** is a first-order reaction:

$$v = k_1[\mathbf{1}]^- \quad (1)$$

the reverse process is of second order:

$$v = k_{-1}[\mathbf{1a}]^-[CO] \quad (2)$$

Therefore, at low concentrations the rate for the forward reaction is high compared to the rate of the reverse reaction; at high concentrations the forward rate is not affected, but the readdition of the CO ligand proceeds faster due to the second-order kinetics.

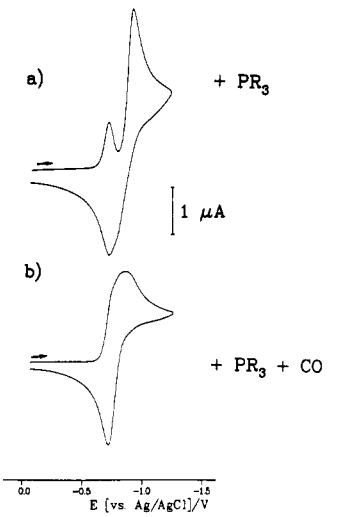

Figure 3. Cyclic voltammograms of 9.0×10^{-4} M **1** in CH_3CN/0.1 M $TBAPF_6$ (a) in the presence of 3.1 mM PPh_3 and (b) after further addition of CO (saturated solution). Scan rate = 0.3 V s^{-1}, T = 24 °C.

Scheme II

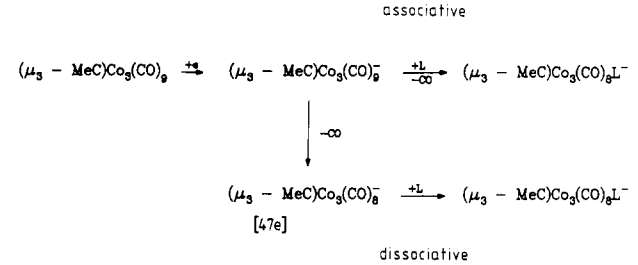

Thus, by simply changing the concentrations of the reacting species or by adding CO to the solution, the process can be switched from the domain of kinetic control into the domain of thermodynamic control. The fast readdition of CO to $[\mathbf{1}]^-$ at high concentrations of **1** renders the decomposition of $[\mathbf{1}]^-$ to $[Co(CO)_4]^-$ impossible.

A further point of controversy becomes clear by these findings. Until now it could not be decided unambiguously whether substitution processes of the anions of tricobalt carbonyl clusters follow a dissociative or an associative pathway[8,16e] (Scheme II). On the basis of the assumption of a stable anion $[\mathbf{1}]^-$,[15b,c] all ligand-substitution processes should occur via an associative mechanism. The detected CO dissociation reaction of $[\mathbf{1}]^-$ in thoroughly dried and purified CH_3CN leading to $[\mathbf{1a}]^-$ as well as all other observations now supplies strong evidence for the existence of the 47-electron species $[\mu_3\text{-}XCo_3(CO)]_8^-$ (X = CMe, CPh), the key intermediates in the dissociative reaction pathway.

Additional support for this view was obtained by reduction experiments with **1** that were carried out in the presence of several added ligands such as PPh_3 or CO. As was already shown by Rieger et al.[8] and Robinson et al.,[16e] the μ_3-$XCo_3(CO)_9$ clusters undergo efficient ETC substitution reactions with PPh_3 to form clusters of the general formula μ_3-$XCo_3(CO)_8PPh_3$. Our voltammetric measurements of **1** in the presence of added PPh_3, which show only a small wave for the reduction of **1**, also illustrate a high efficiency of the ETC route (Figure 3a).[33]

To decide whether the ligand substitution as the rate-determining propagation step is associative or dissociative (Scheme II),

(33) Typical electron transfer chain (=ETC) processes take place when the potential for the reduction of the product is more negative than that of the reactant, which is the case for the reactant **1** ($E^\circ_{1/[1]^-}$ = −0.745 V) and for its PPh_3 substitution product **14** ($E_{4/[4]^-}$ = −0.98 V). As a consequence of this ECE mechanism almost all of the starting material **1** is homogeneously reduced by the rapidly formed anion $[\mathbf{14}]^-$ and the whole process (Scheme II) is catalytic and proceeds via an electron-transfer chain route. Therefore, in the case of an effective electrocatalysis with high turnover numbers the reactant wave in cyclic voltammetry decreases dramatically and may even disappear provided that no side reactions stop the catalytic cycle.

Scheme III

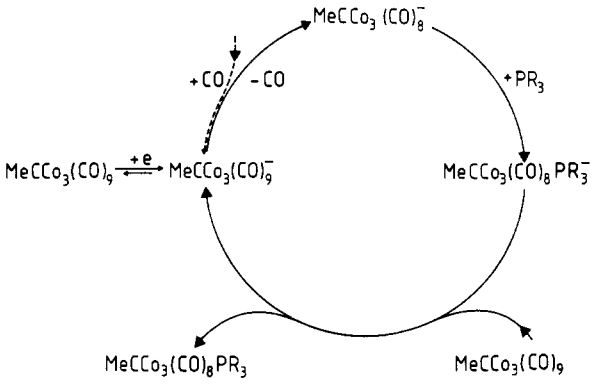

an analysis of the kinetic rate equations is helpful. The associative mechanism is described by a simple second-order rate expression:

$$d[\mathbf{1}^-]/dt = -k_1[\mathbf{1}^-][PPh_3] \quad (3)$$

For the two-step dissociative pathway (Scheme III), from the steady-state approximation the following rate equation results:

$$\frac{d[\mathbf{1}^-]}{dt} = -\frac{k_1k_2[\mathbf{1}^-][PPh_3]}{k_{-1}[CO] + k_2[PPh_3]} \quad (4)$$

Equations 3 and 4 reveal that by increasing the concentration of the departing ligand CO, the rate of the substitution reaction should be significantly lowered only when the process is dissociative. This is exactly what is observed experimentally. In the presence of CO the ETC reaction is efficiently suppressed. By saturation of the solution of **1** and PPh_3 with CO, the electrochemical reduction wave of **1** increases; the product wave is superimposed on it (Figure 3b). We conclude from these results that the associative pathway does not play a significant role in the reductive ETC ligand substitutions of alkylidyne tricobalt carbonyl clusters. An objection to this conclusion is possible reversibility of the associative mechanism, such that excess CO would again suppress the net rate of substitution. However, the very high ETC substitution efficiency in the presence of even low excess phosphine ligand renders this reversible reaction path improbable. Moreover, we will show below that the existence and stability of the 47e intermediate of the dissociative ligand-substitution process can be proved by direct experimental observation.

Electrochemical Studies of $MeCCo_3(CO)_{9-n}(PR_3)_n$. Unlike the results for **1**, cyclic voltammograms for the reduction of the phosphine-substituted tricobalt clusters are rather complex and cannot be interpreted straightforwardly.[16] Nevertheless, typical group trends with respect to the degree of substitution can be extracted from the electrochemical data. To find such regularities, we have studied the redox chemistry of the phosphine-substituted derivatives **11–35**. The characteristic reduction and oxidation potential of **1–35**, as well as their respective anions, obtained by cyclic voltammetry are summarized in Table I. As expected, the reduction potentials are shifted to negative values with increasing number of phosphine ligands and with their increasing basicity ($PPh_3 < PMePh_2 < PMe_2Ph < PMe_3$). A further general point of interest is that the reactivities upon reduction of these compounds increase with increasing number of phosphine ligands. It is obvious that the Lewis-base character of the PR_3 ligands destabilizes the anions of the corresponding clusters. To develop general statements for each respective group of compounds, we will depict a few typical examples and work out the main features of their redox behavior.

A. Electrochemistry of the Monophosphine-Substituted Clusters. (a) Cyclic Voltammetry of μ_3-$MeCCo_3(CO)_8PMe_2Ph$ (12). Figure 4 shows the cyclic voltammograms for the reduction of **12** in CH_3CN. The formation of the anion $[\mathbf{12}]^-$ at $E_{pc} = -1.04$ V is obviously irreversible, which is documented by several overlapping waves on the reverse scan. When the potential is scanned down to −1.50 V, a second partially reversible reduction wave appears at $E_{pc} = -1.375$ V and an additional anodic wave at $E_{pa} = +0.07$ V is observed. The latter can be attributed to the oxidation of $[Co(CO)_4]^-$. By changing the scan rate from 0.05 to 0.5 V s^{-1} the second reduction wave decreases in height relative to the first and the current function $i_p/v^{1/2}$ for the first wave increases from 7.54 to 7.76 $\mu A/(V/s)^{1/2}$ (Figure 4).

Table I. Characteristic Potentials of **1** and Phosphine-Substituted Clusters[a]

compd	E^1_{pc}	E^2_{pc}	E^0_{R/R^-}	E^1_{pa}[d]	E^2_{pa}	E^3_{pa}
1	−0.78[b]		−0.745			
11[b]	−1.04	−1.54	−1.07	−0.95	−0.75[e]	
12[b]	−1.04	−1.38	−1.06	−0.81	−0.75[e]	
13[b]	−1.02	−1.29	−1.03[c]	−0.78	−0.75[e]	
14[b]	−0.94	−1.20	−0.98[c]	−0.71	−0.75[e]	
21	−1.47	−1.90[f]			−1.09	−0.53[e]
22	−1.35	−1.88[f]			−1.07	−0.46[e]
23	−1.29				−0.94	−0.33[e]
31	−1.90				−1.54	−0.94
32	−1.86				−1.46	−0.89
35	−1.76				−1.43	−0.85

[a] Cyclic voltammetry was performed at a Pt electrode (i.d. = 1 mm) with solutions 10^{-3} M in substrate and 0.1 M $TBAPF_6$ for CH_3CN. All potentials are expressed in volts vs Ag/AgCl (calibration with Cp_2Fe/Cp_2Fe^+ couple taken to have 0.352 V in all solvents). Unless noted differently the scan rate was 0.4 V s^{-1} and T = 24 °C. [b] Scan rate = 0.2 V s^{-1}. [c] Standard potentials determined at low temperatures (<0 °C) and high scan rates (≥10 V s^{-1}). [d] Waves visible only as shoulders disappearing at high scan rates. [e] Scan rate = 10 V s^{-1}. [f] Only at temperatures ≤10 °C.

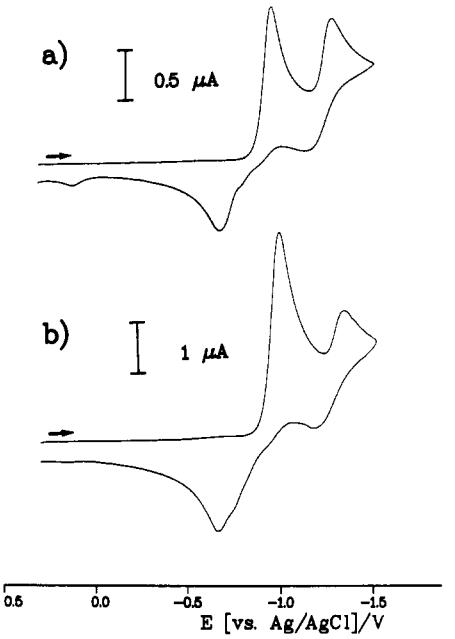

Figure 4. Cyclic voltammograms of 9.0×10^{-4} M **12** in CH_3CN/0.1 M $TBAPF_6$. T = 24 °C. (a) v = 0.05 V s^{-1}; (b) v = 0.5 V s^{-1}.

To eliminate the possibility of CH_3CN being incorporated in the reduced species,[10c,16e] additional measurements were carried out in the noncoordinating solvent CH_2Cl_2.[34] In addition, the concentration of **12** was varied. Cyclic voltammetry reveals nearly identical behavior for both solvents in the cathodic scan, whereas on scan reversal small differences in the peak heights of the waves are observed. More striking is the concentration dependence, which gives a peak current ratio between the first and the second cathodic wave of 5.7 for the low concentration (2.9×10^{-4} M) and of 2.6 for the high concentration (2×10^{-3} M).

Several simple conclusions can be drawn from these semiquantitative observations. The change of the height of the second cathodic wave as a function of both the scan rate and the con-

(34) (a) Bixler, J. W.; Bond, A. M.; Dickson, R. S. *Organometallics* **1986**, *5*, 1435–1441. (b) Boyd, D. C.; Rodman, G. S.; Mann, K. R. *J. Am. Chem. Soc.* **1986**, *108*, 1779–1784.

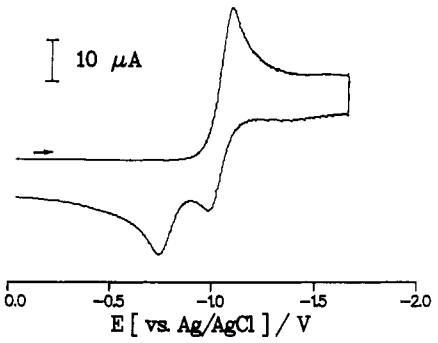

Figure 5. Cyclic voltammograms of 9.0×10^{-4} M **12** in CH_3CN/0.1 M $TBAPF_6$. Scan rate = 50 V s^{-1}. T = 24 °C.

centration of **12** indicates that the species reduced at −1.38 V is formed from the primarily formed anion $[\mathbf{12}]^-$. The concentration dependence of this follow-up reaction proves that the rate-determining step is at least of second order. Moreover, the increase of the current function of the wave at E_{pc} = −1.04 V with increasing scan rates indicates an ETC process that produces the species which is reduced at E_{pc} = −1.38 V. This species has been identified as the PMe_2Ph disubstituted cluster **22** by comparison with CVs of an authentic sample of **22**. The similarity of CV diagrams obtained in CH_3CN and CH_2Cl_2 rules out fast ligand substitution by CH_3CN. This implies that during the reaction of **12** there must be a reaction path, in which the phosphine ligand PMe_2Ph is liberated.

At this level of analysis the following reaction sequences are identified (L = PMe_2Ph):

$$MeCCo_3(CO)_8L\ (\mathbf{12}) \underset{-e}{\overset{+e}{\rightleftharpoons}} [MeCCo_3(CO)_8L]^{\bullet-}\ ([\mathbf{12}]^{\bullet-}) \quad (5)$$

$$[MeCCo_3(CO)_8L]^{\bullet-}\ ([\mathbf{12}]^{\bullet-}) \xrightarrow[-CO]{+L} [MeCCo_3(CO)_7L_2]^{\bullet-}\ ([\mathbf{22}]^{\bullet-}) \quad (6)$$

The ETC reaction is driven by an exergonic redox process between **12** and $[\mathbf{22}]^-$ ($E^\circ_{12/[12]^-} > E^\circ_{22/[22]^-}$):

$$[MeCCo_3(CO)_7L_2]^- + MeCCo_3(CO)_8L \rightleftarrows MeCCo_3(CO)_7L_2 + [MeCCo_3(CO)_8L]^- \quad (7)$$

Additional information on the reduction mechanism of **12** was obtained by using high scan rates and/or low temperatures. Figure 5 shows a cyclic voltammogram of **12** measured at a scan rate of 50 V s^{-1}. Surprisingly, the cathodic wave at E_{pc} = −1.38 V as well as most of the irreversible anodic waves have disappeared and a partly reversible wave for the reduction of **12** has emerged. There is, however, still an oxidation wave at E_{pa} = −0.75 V which remains irreversible under all experimentally accessible conditions.

Similar effects were observed when the temperature was lowered (Figure 6). At −10 °C with a scan rate of 0.5 V s^{-1} the first reduction wave became slightly reversible and the second one had disappeared again, and on the return scan only one irreversible oxidation wave at E_{pa} = −0.75 V was detected (Figure 6a). Raising the scan rate to 50 V s^{-1} yielded a fully reversible cyclic voltammogram (Figure 6c). By the evaluation of the current ratios i_{pa}/i_{pc} in different cyclic voltammograms[35] a first-order rate constant for the follow-up reaction of 7.9 s^{-1} for the anion $[\mathbf{12}]^-$ at −10 °C was determined. Analogously, at −43 °C the rate constant was 0.12 s^{-1}. The rate constants for the follow-up reactions of $[\mathbf{11}]^-$, $[\mathbf{13}]^-$, and $[\mathbf{14}]^-$ were determined by the same technique (Table II, see below).

From these data it is obvious that at the anion level at least two subsequent reactions, a slow one and a fast one, take place, which occur either successively or simultaneously. To gain further insight, we again added an excess of the ligands to the solution. After addition to excess PMe_2Ph to a solution of **12** at −10 °C in methylene chloride, the oxidation wave at −0.75 V had decreased

(35) Nicholson, R. S.; Shain, I. *Anal. Chem.* **1966**, *38*, 1406.

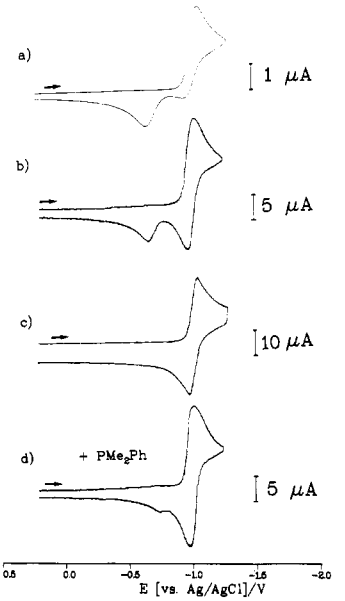

Figure 6. Cyclic voltammograms of **12**. T = −10 °C. (a) 1.0×10^{-3} M in CH_3CN/0.1 M $TBAPF_6$, v = 0.5 V s^{-1}; (b) 2.0×10^{-3} M in CH_2Cl_2/0.1 M $TBABF_4$, v = 5 V s^{-1}; (c) 1.0×10^{-3} M in CH_3CN/0.1 M $TBAPF_6$, v = 50 V s^{-1}; (d) 2.0×10^{-3} M in CH_2Cl_2/0.1 M $TBABF_4$, v = 5 V s^{-1}, with 3.0×10^{-2} M PMe_2Ph.

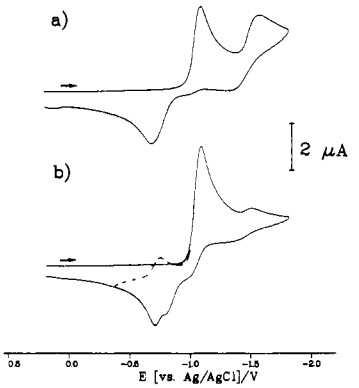

Figure 7. Cyclic voltammograms of 1.0×10^{-3} M **11** in CH_3CN/0.1 M $TBAPF_6$. T = 24 °C. Scan rate = 0.4 V s^{-1}. (a) Without CO; (b) solution saturated with CO; dashed line, second forward sweep (E_λ = −0.4 V).

in magnitude and the reversibility of the formation of the radical anion $[\mathbf{12}]^-$ had increased (Figure 6d).

From these observations it becomes evident that (a) the radical anion $[\mathbf{12}]^-$ eliminates PMe_2Ph in a fast chemical follow-up step and (b) the same ligand is added again to the 47e intermediate in a slow reverse reaction. In the presence of additional CO at the same temperature (−10 °C) no change of the voltammetric response is registered. However, at room temperature the excess ligand CO efficiently suppresses the ETC reaction with the phosphine ligand, which is indicated by the decrease of the signal at E_{pc} = −1.38 V and the increase of the reduction wave of **12** at E_{pc} = −1.04 V. The reverse scan now shows an anodic wave at E_{pa} = −0.69 V, which can unambiguously be correlated with the $\mathbf{1}/[\mathbf{1}]^-$ redox pair additionally documented by the appearance of a cathodic peak at E_{pc} = −0.760 V in a successive scan. Figure 7 shows cyclic voltammograms of this crucial experiment for the cluster **11**. As can be seen, after the addition of CO the reduction wave for the ETC product **21** at E_{pc} = −1.54 V decreases, while the signal for the starting material at E_{pc} = −1.04 increases. Furthermore, the waves for the reversible redox pair $\mathbf{1}/[\mathbf{1}]^-$ are clearly discernible.

Applying the arguments given by the rate equations (3) and (4), one again is led to the conclusion that the ETC reaction is dissociative, CO being eliminated in the first step and the phos-

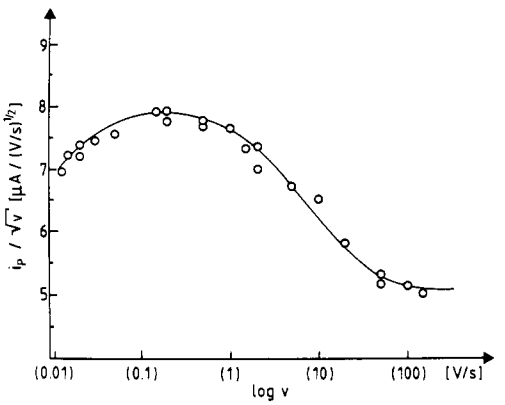

Figure 8. Plot of the first cathodic peak current function of **12** vs log v (c = 9.0 × 10^{-4} M, CH_3CN/0.1 M $TBAPF_6$, T = 24 °C).

phine ligand that must derive from a competing elimination reaction being added in the second step. Our knowledge of the reaction pattern of $[\mathbf{12}]^-$ now comprises the following chemical steps:

$$[MeCCo_3(CO)_8L]^{\bullet-}\ ([\mathbf{12}]^{\bullet-}) \xrightarrow{\text{slow}} [MeCCo_3(CO)_7L]^{\bullet-}\ ([\mathbf{12a}]^{\bullet-}) + CO \quad (8)$$

$$[MeCCo_3(CO)_8L]^{\bullet-}\ ([\mathbf{12}]^{\bullet-}) \underset{\text{slow}}{\overset{\text{fast}}{\rightleftharpoons}} [MeCCo_3(CO)_8]^{\bullet-}\ ([\mathbf{1a}]^{\bullet-}) + L \quad (9)$$

$$[MeCCo_3(CO)_7L]^{\bullet-}\ ([\mathbf{12a}]^{\bullet-}) + L \rightarrow [MeCCo_3(CO)_7L_2]^{\bullet-}\ ([\mathbf{22}]^{\bullet-}) \quad (10)$$

$$[MeCCo_3(CO)_8]^{\bullet-}\ ([\mathbf{1a}]^{\bullet-}) + CO \rightarrow [MeCCo_3(CO)_9]^{\bullet-}\ ([\mathbf{1}]^{\bullet-}) \quad (11)$$

Nevertheless, there is one point that needs further explanation. The low-temperature experiments show an irreversible anodic wave at E_{pa} = −0.75 V which cannot be assigned to the oxidation of one of the already known reduction products of **12**. This wave is also visible in the room-temperature experiments but is partly hidden by the oxidation wave of $[\mathbf{1}]^-$ which is formed from $[\mathbf{12}]^-$ by the elimination of the phosphine ligand and the subsequent addition of CO (eq 9 and 11). The voltammetric data obtained at −10 °C in the presence of an excess of PMe_2Ph (Figure 6d) confirm that the species reoxidized at E_{pa} = −0.75 V must be a follow-up product of the phosphine elimination from $[\mathbf{12}]^-$. The nature of this product is clarified by the study of the current function of the reduction of **12** as a function of the sweep rate (Figure 8).

Surprisingly, the current function increases up to a scan rate of 0.5 V s^{-1} and then decreases significantly down to a plateau value at 100 V s^{-1}. Normally, for a pure ETC reaction which suppresses the heterogeneous charge transfer of the $\mathbf{12}/[\mathbf{12}]^-$ redox couple in favor of homogeneous reactions, one would expect an increase of the current function only with rising scan rate. As the CO elimination, the initial rate-determining step for this process, is slow, at sweep rates above 1 V s^{-1} almost no further electrocatalytic ligand substitution takes place and the current function should stay constant. The fact that it decreases again above 1 V s^{-1} is characteristic of a competing ECE mechanism that involves two one-electron steps separated by a chemical step.[36] The voltammetric data obtained after the addition of the PMe_2Ph ligand have already shown (Figure 6d) that the primarily formed 49e radical anion $[\mathbf{12}]^-$ eliminates a phosphine ligand in a fast but reversible chemical follow-up step, yielding the 47e species $[MeCCo_3(CO)_8]^-$. Obviously, this intermediate can be reduced further to the dianion $[MeCCo_3(CO)_8]^{2-}$, which is a closed-shell 48e configuration cluster and may therefore be relatively stable:

$$[MeCCo_3(CO)_8]^{\bullet-}\ ([\mathbf{1a}]^{\bullet-}) \underset{-e}{\overset{+e}{\rightleftharpoons}} [MeCCo_3(CO)_8]^{2-}\ ([\mathbf{1a}]^{2-}) \quad (12)$$

Its reoxidation in the reverse sweep at E_{pa} = −0.75 V leads back to the 47e intermediate which reacts preferentially with the free phosphine ligand (eq 9) with the formation of $[\mathbf{12}]^-$.

(b) Cyclic Voltammetry of μ_3-$MeCCo_3(CO)_8PPh_3$ (14). Additional features of the $MeCCo_3(CO)_8L$ redox system were clarified by the study of the PPh_3 compound **14**. The cathodic reduction of **14** carried out at room temperature[15a,c] seems to be quite reversible (Figure 9a), the amount of **24** formed via ETC catalysis being small and the peak separation of the waves for the first redox process amounting only to 120 mV. Experiments at low temperatures now showed, however, that the radical anion of **14** obviously disappears in a fast chemical reaction and the initially observed reversibility is an artifact. The reoxidation wave of the $\mathbf{14}/[\mathbf{14}]^-$ redox couple becomes only visible at low temperatures (−43 °C) when a scan rate of at least 150 V s^{-1} is applied (Figure 9b,c).

Under these conditions the irreversible oxidation wave is still observed and dominates at lower scan rates in the range between −0.75 and −0.45 V. Cyclic voltammetry of mixtures of **14** and **12** reveals that the anodic wave at E_{pa} = −0.75 V resulting from the products of the fast follow-up reaction represents the oxidation

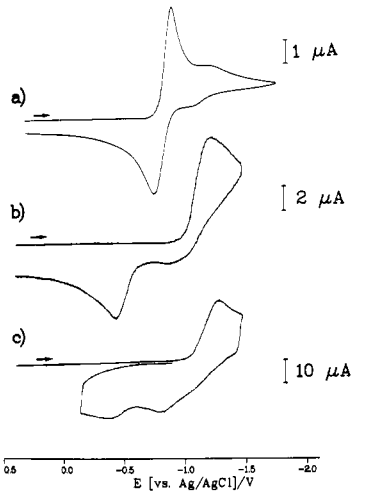

Figure 9. Cyclic voltammograms of 9.4 × 10^{-4} M **14** in CH_3CN/0.1 M $TBAPF_6$. (a) v = 0.3 V s^{-1}, T = 24 °C; (b) v = 10 V s^{-1}, T = −43 °C; (c) v = 150 V s^{-1}, T = −43 °C.

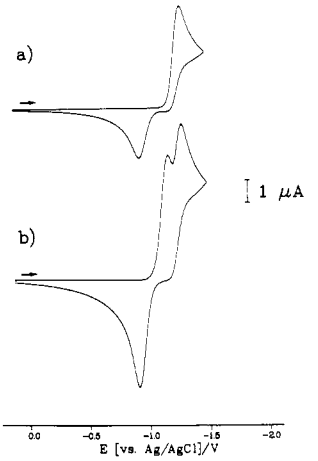

Figure 10. Comparison of the reduction products of **12** and **14** by cyclic voltammetry: scan rate = 0.2 V s^{-1}, T = −10 °C, CH_2Cl_2/0.1 M $TBABF_4$. (a) 1.6 × 10^{-3} M **12**; (b) 1.6 × 10^{-3} M **12** + 1.5 × 10^{-3} M **14**.

(36) (a) Nicholson, R. S.; Shain, I. *Anal. Chem.* **1965**, *37*, 178–190. (b) Saveant, J. M. *Electrochim. Acta* **1967**, *12*, 753–766.

Table II. First-Order Rate Constants and Activation Parameters for the Phosphine Elimination from the 49-Electron Anionic $MeCCo_3(CO)_8PR_3$

	k,[a] s^{-1}			$\Delta H^{\ddagger}$,	$\Delta S^{\ddagger}$,
	24 °C	−10 °C	−43 °C	kJ mol^{-1}	eu
11	27	1.1	0.07	49	−50
12	232	7.9	0.12	64	9
13	500	43.5	1.0	52	−22
14			77		

[a] Determined from the i_{pa}/i_{pc} ratios according to the method of Nicholson.[34] In the voltammograms studied the CO elimination has no effect since the scan rates are greater than 10 V/s.

of an identical species (Figure 10).

The same holds true for all other monosubstituted clusters (Table I). This is a further proof of the proposed reaction scheme in which the fast elimination of a phosphine ligand from the cluster anion produces the identical intermediate $[MeCCo_3(CO)_8]^-$ and subsequently the dianion $[MeCCo_3(CO)_8]^{2-}$, in every case.

B. Kinetics and Mechanisms of Ligand Substitution for the Monosubstituted Clusters. Although the puzzling variety of voltammetric curves obtained during the reductions of **11–14** gives the impression that these processes create a mixture of numerous products which may also imply the destruction of the metal framework, our discussion has now reached a level which offers a relatively simple mechanistic picture. In principle, there are two main reaction pathways, one of which is based on a fast reversible phosphine elimination from the electrochemically generated cluster anion (eq 9) the other one on a slow reversible CO elimination (eq 8). The apparent complexity of the subsequent pattern results from the fact that both PR_3 and CO may be added to the two different 47e intermediates, thus either initiating an ETC catalysis (eq 7 and 10) or producing the radical anion of $[\mathbf{1}]^-$ (eq 11). In those cases where the CO elimination is very slow or the voltammetric time scale is short, the reactive 47e intermediate is stabilized by further reduction to a 48e species (eq 12). These unambiguous findings rule out other frequently discussed mechanisms such as isomerization[8,9e,10b,c] of the cluster anion or even destruction of the metal framework.

The evaluation of the kinetic data at different temperatures allows the construction of Arrhenius plots. The resulting activation parameters are summarized in Table II. The low activation enthalpies indicate a weak Co–P bond, while the small entropy values are typical for a dissociative ligand substitution mechanism.[37] These findings are in full agreement with the other experimental data showing that PR_3 and CO are very labile ligands.

The main differences in the voltammetric behavior among the monophosphine-substituted clusters result preferentially from their differing kinetics. As a rule, the rate of phosphine elimination increases in the order $PMe_3 < PMe_2Ph < PMePh_2 < PPh_3$ (Table II). The inverse dependency holds for the rate of the competing CO elimination. It is well-known that substitution of CO by the less strong π-acid PR_3 renders the remaining metal–carbonyl bonds stronger.[38]

Normally, the decreasing basicity on passing from PMe_3 to PPh_3 should cause an increase of the stability of the respective neutral clusters and especially of the corresponding radical anions. On the other hand, the steric demands of the phosphine ligands increase from PMe_3 to PPh_3. The experimental results (Table II) prove that the destabilization must be mainly related to steric rather than electronic factors. There is some further evidence for this interpretation. In case of the sterically less demanding but strongly basic PMe_3 even a tetrasubstituted derivative is known.[39] For the bulkier but less basic PMe_2Ph the maximum degree of substitution is 3, while for PPh_3 the trisubstituted derivative is unknown, and the very labile disubstituted derivative has been synthesized only very recently by carefully ETC-catalyzed ligand substitution.[16d]

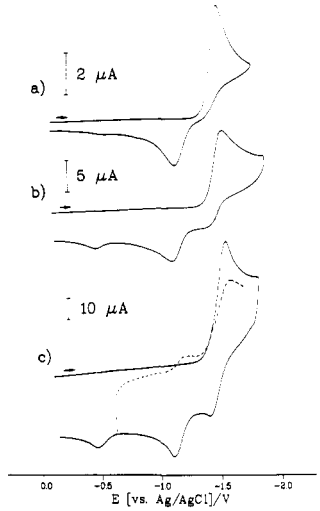

Figure 11. Cyclic voltammograms of 9.2×10^{-4} M **21** in CH_3CN/0.1 M $TBAPF_6$. T = 24 °C. (a) v = 0.4 V s^{-1}; (b) v = 50 V s^{-1}; (c) v = 150 V s^{-1}; dashed line, second forward sweep (E_λ = −0.7 V).

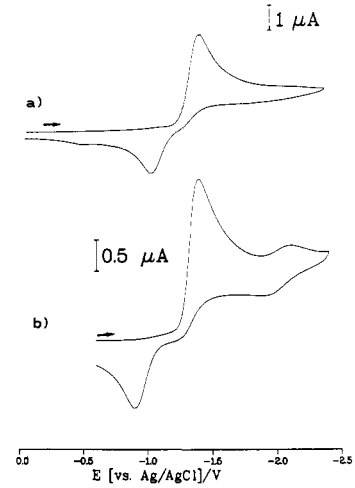

Figure 12. Cyclic voltammograms of 9.2×10^{-4} M **21** in CH_3CN/0.1 M $TBAPF_6$. Scan rate: 0.2 V s^{-1}. (a) T = 24 °C; (b) T = −10 °C.

C. Voltammetry of the Bisphosphine-Substituted Clusters. At a first glance, the electrochemistry of the disubstituted tricobalt carbonyl cluster differs significantly from that of the monosubstituted derivatives (Table I). Figure 11 presents cyclic voltammograms for the reduction of **21** in CH_3CN recorded with different scan rates, which are typical for this whole group of compounds. Applying a scan rate of 0.4 V s^{-1}, the cathodic scan shows only a single large wave with a peak potential (E_{pc}) of −1.47 V. Upon scan reversal a smaller oxidation wave with an anodic peak potential (E_{pa}) of −1.09 V is observed. At room temperature no further cathodic waves are visible. Therefore, under these conditions an ETC process leading to a phosphine-trisubstituted complex can be excluded.

Raising the scan rate to 50 V s^{-1} and more leads to a significant decrease of the peak current function for the reduction of **21** and produces in the reverse scan a further oxidation wave at E_{pa} = −0.47 V. In addition, the wave for the reoxidation of the initially formed radical anion $[\mathbf{21}]^-$ can be observed at scan rates above 100 V s^{-1}. Moreover, a second cathodic sweep or multisweep experiments at 150 V s^{-1} show further small cathodic waves at E_{pc} = −1.25 V, which are coupled with the anodic waves at E_{pa} ≈ −1.09 V, thus indicating an increasing chemical reversibility of the corresponding redox process. Simultaneously with this phenomenon, the height of the anodic wave at E_{pa} = −0.47 V also

(37) (a) Basolo, F.; Pearson, G. P. *Mechanisms of Inorganic Reactions*; Wiley: New York 1967. (b) Schmid, R.; Sapunov, V. N. *Nonformal Kinetics*; Verlag Chemie: Weinheim, 1982.
(38) Shriver, D. F. *J. Organomet. Chem.* **1975**, *94*, 259–271.
(39) Beurich, H.; Vahrenkamp, H., unpublished.

increases (Figure 11c). This gives evidence for the assumption that the products of both oxidation steps at −1.09 and −0.47 V belong to the same reaction path. Similar effects are obtained when the temperature is lowered. As expected, the rates of the successive chemical steps decrease, and consequently the waves for the follow-up products disappear at relatively low scan rates. Surprisingly, at temperatures below 0 °C an additional cathodic wave at $E_{pc} = -2.0$ V can be observed, the potential of which is nearly identical with that of the reduction of **31** (see below; Figure 12).

The decrease of the current function of the first reduction wave with increasing scan rate as well as the appearance of an oxidation wave for a follow-up product is characteristic of an ECE mechanism,[36] i.e., a chemical reaction that is coupled between two electron-transfer steps. In analogy to the findings with the monosubstituted clusters, we assume that the radical anion $[\mathbf{21}]^-$ eliminates the phosphine ligand producing the 47e intermediate $[MeCCo_3(CO)_7L]^-$ ($[\mathbf{11a}]^-$), which is immediately reduced to the stable 48e dianion $[MeCCo_3(CO)_7L]^{2-}$ ($[\mathbf{11a}]^{2-}$). The reoxidation of this reaction product takes place at $E_{pa} = -1.09$ V. This is similar to the oxidation potential of the follow-up product of $[\mathbf{11}]^-$ after the elimination of CO.

There are two possibilities for the further reaction of $[\mathbf{11a}]^-$ generated as above at −1.09 V. In analogy to eq 10 the anion may pick up the phosphine ligand, re-forming the anion $[\mathbf{21}]^-$, which at the actual potential ($E(t) > E^\circ_{\mathbf{21}/[\mathbf{21}]^-}$) is immediately reoxidized to the neutral species **21**. This process (eq 13 and 14), the reverse reaction of the elimination, is slow and can only be observed at low scan rates.

$$[MeCCo_3(CO)_7L]^{\bullet-}\ ([\mathbf{11a}]^{\bullet-}) + L \xrightarrow{\text{slow}} [MeCCo_3(CO)_7L_2]^{\bullet-}\ ([\mathbf{21}]^{\bullet-}) \quad (13)$$

$$[MeCCo_3(CO)_7L_2]^{\bullet-}\ ([\mathbf{21}]^{\bullet-}) \underset{+e}{\overset{-e}{\rightleftharpoons}} MeCCo_3(CO)_7L_2\ (\mathbf{21}) \quad (14)$$

Consequently, an irreversible oxidation wave appears at $E_{pa} = -1.09$ V (ECE mechanism). On the other hand, at high scan rates the 47e intermediate $[\mathbf{11a}]^-$ cannot react with the phosphine ligand owing to the small rate constant. Thus, when the potential is scanned still more positively, it is transformed at $E_{pa} = -0.47$ V into the neutral 46e intermediate **11a**, which becomes stabilized by the fast readdition of a phosphine ligand still present in the diffusion layer of the electrode (eq 15 and 16, EEC mechanism). When the anodic scan is reversed at $E_\lambda = -0.8$ V, the 47e species $[\mathbf{11a}]^-$ still exists and can again be reduced to the 48e dianion $[\mathbf{11a}]^{2-}$ (Figure 11c).

$$[MeCCo_3(CO)_7L]^{\bullet-}\ ([\mathbf{11a}]^{\bullet-}) \underset{+e}{\overset{-e}{\rightleftharpoons}} MeCCo_3(CO)_7L\ (\mathbf{11a}) \quad (15)$$

$$MeCCo_3(CO)_7L\ (\mathbf{11a}) + L \xrightarrow{\text{fast}} MeCCo_3(CO)_7L_2\ (\mathbf{21}) \quad (16)$$

The arguments for the different reaction pathways are fully consistent with the experimental data. Further support for this interpretation can be gained from the results obtained with the trisubstituted clusters.

A further detail of the reduction mechanism of **21** is gained from low-temperature experiments. As already mentioned, although the rates of follow-up reactions decrease with diminishing temperatures, a new cathodic wave appears below 0 °C at −2.0 V, indicating the formation of the trisphosphine-substituted cluster **31**. As the redox potential of the $\mathbf{31}/[\mathbf{31}]^-$ couple lies negative to that of the $\mathbf{21}/[\mathbf{21}]^-$ couple, this process is obviously ETC catalyzed. The fact that this ETC sequence initiated by CO elimination is observed only at low temperatures—and this is true for all disubstituted clusters—proves that the activation energy for the CO elimination is lower than that for the phosphine elimination. Therefore, at room temperature the phosphine elimination dominates, while at low temperatures there is a competition between both reaction paths.

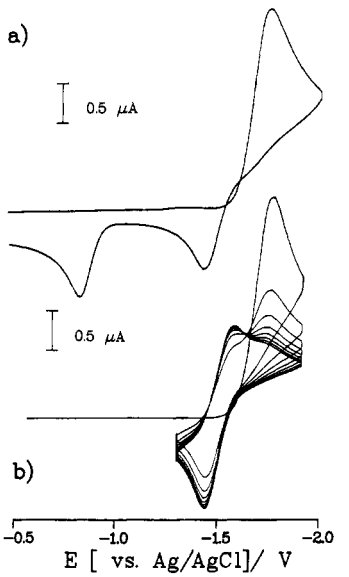

Figure 13. Cyclic voltammograms of 8.0×10^{-4} M **35** in CH_3CN/0.1 M $TBAPF_6$. scan rate: 0.4 V s^{-1}. $T = 24$ °C. (a) Single sweep cyclic voltammogram; (b) multisweep cyclic voltammogram scanned between −1.25 and −1.85 V.

D. Electrochemistry of the Trisphosphine-Substituted Clusters. The slow-scan cyclic voltammetric behavior of the trisubstituted clusters **31**, **32**, and **35** (Table I) is similar to the results obtained at high scan rates for the disubstituted complexes. Moreover, it resembles in all essential details the cyclic voltammetric behavior for the reduction of the phosphido-bridged rhodium complex $[Rh(\mu\text{-}tBu_2P)(CO)_2]_2$[40] and the oxidation of the 5,6-dihydrobenzocinnoline system.[22] All these examples show ECE/EEC type mechanisms.

(a) Voltammetry of μ_3-$MeCCo_3(CO)_6(PEt_2Ph)_3$ (35). A typical cyclic voltammogram representing the reduction of **35** is given in Figure 13a. In the forward scan a large cathodic wave at $E_{pc} = -1.76$ V is observed, followed in the reverse scan by two smaller oxidation waves at peak potentials of −1.43 and −0.85 V. A striking feature of this curve is the trace crossing that appears upon scan reversal, indicating that a reducible species is produced during the anodic scan.

In a multisweep experiment scanned between −1.25 and −1.85 V a new reduction wave with a cathodic peak potential (E_{pc}) of −1.59 V appears in the second cathodic scan (Figure 13b). Simultaneously, the original cathodic wave at $E_{pc} = -1.76$ V decreases in height. In subsequent scans the waves at $E_{pa} = -1.43$ V and $E_{pc} = -1.58$ V, which obviously represent the oxidation and the reduction of a stable redox couple, increase further while the original cathodic wave gradually disappears. A steady-state level is reached after about nine cycles. In the same experiment, in addition to the unusual trace crossing effect, an isopotential point (IPP) is observed at −1.61 V. This phenomenon can be interpreted in complete analogy to an isosbestic point. It proves that the transformation of an electroactive species into another one occurs without side reactions and quantiatively.[25] Although IPPs have been known for adsorbed species and polymer films since 1972, only very recently have they been described for systems where both reactants and products are in solution.[40,41]

As already demonstrated by the behavior of **21**, the large reduction wave of **35** is characteristic for an ECE mechanism that involves as a chemical step the elimination of a phosphine ligand from $[\mathbf{35}]^-$. The resulting 47e intermediate $[\mathbf{25a}]^-$ is stabilized by a further reduction step to yield the 48e species $[\mathbf{25a}]^{2-}$ (eq 17–19).

(40) Gaudiello, J. G.; Wright, T. C.; Jones, R. A.; Bard, A. J. *J. Am. Chem. Soc.* **1985**, *107*, 888–897.
(41) Heinze, J.; Dietrich, M.; Hinkelmann, K.; Meerholz, K.; Rashwan, F. *DECHEMA-Monog.* **1989**, *112*, 61–74.

$$MeCCo_3(CO)_6L_3\ (\mathbf{35}) \underset{-e}{\overset{+e}{\rightleftharpoons}} [MeCCo_3(CO)_6L_3]^{\bullet-}\ ([\mathbf{35}]^{\bullet-}) \quad (17)$$

$$[MeCCo_3(CO)_6L_3]^{\bullet-}\ ([\mathbf{35}]^{\bullet-}) \xrightarrow{fast} [MeCCo_3(CO)_6L_2]^{\bullet-}\ ([\mathbf{25a}]^{\bullet-}) + L \quad (18)$$

$$[MeCCo_3(CO)_6L_2]^{\bullet-}\ ([\mathbf{25a}]^{\bullet-}) \underset{-e}{\overset{+e}{\rightleftharpoons}} [MeCCo_3(CO)_6L_2]^{2-}\ ([\mathbf{25a}]^{2-}) \quad (19)$$

During the voltammetric reoxidation the system is transformed by two successive one-electron steps into a neutral 46e intermediate to which the ligand that was liberated before is re-added, regenerating the starting material (EEC mechanism, eq 19–21).

$$[MeCCo_3(CO)_6L_2]^{\bullet-}\ ([\mathbf{25a}]^{\bullet-}) \underset{+e}{\overset{-e}{\rightleftharpoons}} MeCCo_3(CO)_6L_2\ (\mathbf{25a}) \quad (20)$$

$$MeCCo_3(CO)_6L_2 + L\ (\mathbf{25a}) \xrightarrow{fast} MeCCo_3(CO)_6L_3\ (\mathbf{35}) \quad (21)$$

The rate constant for this chemical step must be relatively large since no peak corresponding to the reduction of the 46e intermediate was observed in the second forward sweep at scan rates up to 100 V s^{-1}.

Changing the sweep rates and/or the temperatures does not produce any new signals in the voltammetric response of **35**. This proves that owing to the high kinetic lability of the phosphine ligands, only phosphine elimination occurs and no competitive reactions, especially no CO elimination, take place. Although there are spectacular similarities between the cyclic voltammograms of **35** and those of the phosphido-bridged rhodium complex $[Rh(\mu\text{-}t\text{-}Bu_2P)(CO)_2]_2$[40] and the 5,6-dihydrobenzocinnoline derivatives,[22] in which case the chemical steps have been identified as intramolecular rearrangements, the equivalence concerns only the type of electrochemical reaction mechanisms (ECE, EEC) and not the nature of the respective chemical reactions.

It could be shown by two additional independent experiments that phosphine is, in fact, eliminated during the reductions of trisphosphine-substituted clusters: In the first case we exploited the finding discussed before that **1** reacts with free phosphine ligands, PR_3, via an ETC-catalyzed reaction to form clusters of the general composition $(\mu_3\text{-MeC})Co_3(CO)_8(PR_3)$. Indeed, cyclic voltammetry of solutions containing both **1** and **32** demonstrated the formation of **12**. Because in the forward scan the reduction of **32** and therefore the release of the phosphine ligand starts only after the reduction of **1**, the substitution product **12**, formed from **1**, can be detected only in the reverse scan as well as during the second cathodic sweep. In control experiments in which only **1** was present in solution, there was no evidence in the voltammograms for the formation of any decomposition products.

In the second case further evidence for the phosphine ligand elimination reaction from $[\mathbf{35}]^-$ and its re-addition to $[\mathbf{25a}]^-$ is provided by voltammetric experiments with **35** in the presence of a large excess of its phosphine ligand PEt_2Ph. The cathodic scan remains unchanged; however, in the reverse anodic scan the wave at $E_{pa} = -0.85$ V corresponding to the reoxidation of the 47e anion $[\mathbf{25a}]^-$ to the neutral 16e intermediate **25a** disappears and in the second cathodic scan the reduction wave at $E_{pc} = -1.58$ V, which belongs to the normally stable redox pair $[\mathbf{25a}]^-/[\mathbf{25a}]^{2-}$, also disappears (Figure 14).

In view of the foregoing results this experiment shows that after the reoxidation of $[\mathbf{25a}]^{2-}$ to $[\mathbf{25a}]^-$, the phosphine ligand adds slowly to the 47e species $[\mathbf{25a}]^-$, thus re-forming $[\mathbf{35}]^-$. As the actual potential $E(t)$ of the voltammetric sweep at the electrode under these conditions is positioned positively to $E^1_{pc} = -1.76$ V, which itself is more positive than $E^\circ_{\mathbf{35}/[\mathbf{35}]^-}$, $[\mathbf{35}]^-$ is immediately transformed to **35**. This backward reaction becomes dominant because, after the reoxidation of $[\mathbf{25a}]^{2-}$ to $[\mathbf{25a}]^-$, the reaction sequence $\mathbf{35} \rightarrow [\mathbf{35}]^- \rightarrow [\mathbf{25a}]^-$ can no longer occur owing to an electrode potential essentially more positive than $E^\circ_{\mathbf{35}/[\mathbf{35}]^-}$, and therefore the re-addition of the phosphine ligand, despite a small

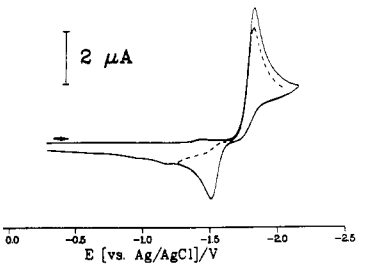

Figure 14. Cyclic voltammogram of 8.0×10^{-4} M **35** in the presence of a 35-fold excess of PEt_2Ph. $T = 24$ °C. Scan rate: 0.4 V s^{-1}. Dashed line: second forward sweep ($E_\lambda = -1.25$ V).

Scheme IV

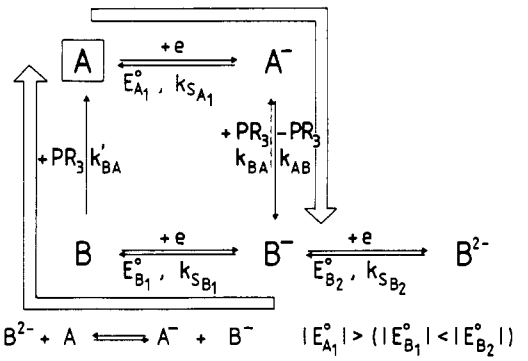

rate constant k_{-1}, is the only occurring process. Normally, in the usual voltammetric experiment in which a low concentration of the phosphine ligand is released during the scan in the potential range negatively to E^1_{pc}, this second-order reaction is negligibly slow.

The redox behavior of the trisphosphine-substituted clusters in cyclic voltammetric experiments can now be described by the following general scheme given in Scheme IV.

In the cathodic scan the starting 48e species **A** (**A** = **31**, **32**, **35**) is reduced via an ECE-type mechanism to $[\mathbf{B}]^{2-}$ (**B** = **21a**, **22a**, **25a**), since the reduction of $[\mathbf{B}]^-$ to $[\mathbf{B}]^{2-}$ is thermodynamically more favorable than that of **A** to $[\mathbf{A}]^-$ ($E^\circ_{B_2} > E^\circ_{A_1}$). Therefore, in the cathodic scan only a single 2e reduction wave is observed. On account of the PR_3 elimination, the resulting stable reduction product $[\mathbf{B}]^{2-}$ is again a 48e species. In the reverse scan $[\mathbf{B}]^{2-}$ is first oxidized to the fairly stable 47e intermediate $[\mathbf{B}]^-$, which at more positive potentials ($E^\circ_{B_1} > E^\circ_{B_2}$) is then oxidized to the neutral 46e intermediate **B**, which in turn re-adds the cleaved PR_3 ligand still present in the diffusion layer in front of the electrode.

The neutral species **B** corresponds to the classical 46-electron intermediate involved in thermal dissociative ligand substitution. As shown in the preceding discussion, the 47-electron intermediate $[\mathbf{B}]^-$ is of analogous significance for the dissociative ETC reaction scheme.[8,9c,11b,16] Until now, evidence for the existence of such a species, formed by one-electron reduction and ligand elimination, was gained only on the basis of kinetic data or product distributions.[8,9d,16] The multisweep voltammetric measurements (Figure 13b) carried out with trisphosphine-substituted derivatives clearly show that the $[\mathbf{B}]^-/[\mathbf{B}]^{2-}$ (=47e/48e) couples are stable on a voltammetric time scale. This holds for both forms of the couple since no decay of the steady-state current was observed after a fairly long period of continuous cycling (ca. 5 min). Our experiments unambiguously reveal that this 47e species not only exists as a short-lived intermediate but may possess considerable stability, provided that donor ligands such as phosphines relieve the electron deficiency and help to shield the unsaturated species by their steric bulk.

The unusual crossover effect observed in the cyclic voltammograms of the trisphosphine-substituted clusters (Figure 13) reveals another important detail of the reaction mechanism. As already mentioned, this phenomenon indicates that after switching of the scan direction, during the reoxidation a cathodic current

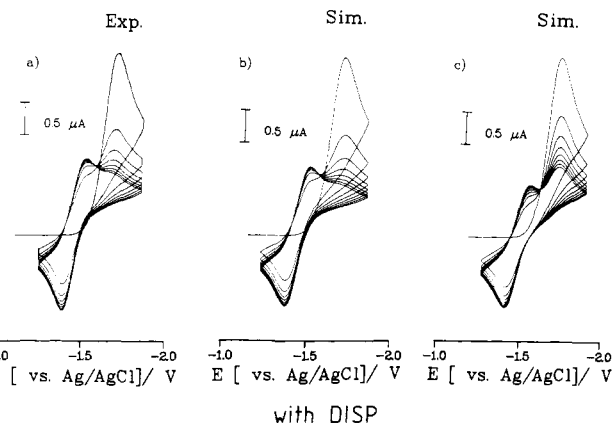

Figure 15. Experimental and simulated cyclic voltammograms of **35**. Simulation data: $C^* = 8 \times 10^{-4}$ M, $E^\circ_{A_1} = -1.66$ V, $E^\circ_{B_2} = -1.49$ V, $k_{s(A_1)} = 1.7 \times 10^{-3}$ cm s^{-1} ($\alpha = 0.55$), $k_{s(B_2)} = 2.6 \times 10^{-3}$ cm s^{-1} ($\alpha = 0.52$), $D = 2.1 \times 10^{-6}$ cm^2 s^{-1}, $k_{AB} = 180$ s^{-1}, $k_{BA} = 20$ M^{-1} s^{-1}, electrode area $= 7.9 \times 10^{-3}$ cm^2, $v = 400$ mV s^{-1}, $E_{\lambda_1} = -1.85$ V, $E_{\lambda_2} = -1.25$ V. (a) Experiment (see Figure 13); (b) ECE/EEC disproportionation mechanism, disproportionation reaction in dynamic equilibrium; (c) ECE/EEC mechanism.

passes through the electrode. Consequently, under the given conditions a diffusion gradient for a reducible species must exist in front of the working electrode. This cannot be explained on the basis of the simple ECE/EEC mechanism. On the contrary, an additional reaction must occur. As outlined in the literature,[42] a homogeneous disproportionation reaction between $[\mathbf{B}]^{2-}$ and **A** producing $[\mathbf{A}]^-$ and $[\mathbf{B}]^-$ would cause such effects (eq 22).

$$[\mathbf{B}]^{2-} + \mathbf{A} \rightleftarrows [\mathbf{B}]^- + [\mathbf{A}]^- \quad (22)$$

Although the forward reaction (22) is not favored thermodynamically ($E^\circ_{A_1} < E^\circ_{B_2}$), it occurs since, owing to the fast elimination of the phosphine ligand, $[\mathbf{A}]^-$ is converted to $[\mathbf{B}]^-$ and will be thus withdrawn from the equilibrium.

Formally, reaction 22 can be simplified to reaction 23 on account of the fast transformation of $[\mathbf{A}]^-$ to $[\mathbf{B}]^-$.

$$[\mathbf{B}]^{2-} + \mathbf{A} \rightleftarrows 2[\mathbf{B}]^- + PR_3 \quad (23)$$

Thermodynamic considerations reveal that for this process the equilibrium must lie to the right. The radical anion $[\mathbf{B}]^-$, continuously formed by reaction 23 in the diffusion layer of the working electrode, is the species that can be once again reduced at the electrode provided that the actual electrode potential $E(t)$ is more negative than $E^\circ_{B_2}$. This is exactly the case in the range of the crossover effect.

(b) Digital Simulation. Further proof for this interpretation was gained by digital simulation of the multisweep voltammogram of **35** (Figure 13b), using the implicit Crank–Nicholson technique.[32] Good simulations require a knowledge of the E° values, the homogeneous and heterogeneous rate constants, and the diffusion coefficients. $E^\circ_{B_2}$ was taken as the average of $E^2_{pc} + E^2_{pa}$ of the $[\mathbf{25a}]^-/[\mathbf{25a}]^{2-}$ couple. The heterogeneous rate constant $k_{s(B_2)}$ for the same couple was determined from the scan-rate dependence of ΔE_p.[43] $E^\circ_{A_1}$ was estimated from the peak potential E^1_{pc}, and the homogeneous first-order rate constant according to the method of Nicholson and Shain.[44] The corresponding heterogeneous rate constant was set at a value similar to that of the $[\mathbf{25a}]^-/[\mathbf{25a}]^{2-}$ couple. The diffusion coefficients, assumed equal for all species, were determined from the peak current of the first reduction wave in the cyclic voltammograms of **35**. For the disproportionation reaction a dynamic equilibrium was assumed. To optimize the simulation a reliable value of the homogeneous chemical rate constant k_{AB} was selected and then varied until the simulated and the experimental cyclic voltammograms were in close agreement. The complexity of the experimental voltammogram (Figure 15a) implies, however, that only a limited variation of the values of the selected parameters is possible.

Figure 15b represents a simulated multisweep voltammogram for the ECE/EEC disproportionation mechanism obtained with the use of the parameters listed in the figure caption. The excellent agreement between the experiment and the simulation proves the correctness of the proposed mechanistic model. Even details such as the position of the isopotential point (IPP) and the extent of the trace crossing are accurately reproduced. Additional simulations show that the crossing over effect is also influenced by the rates of the heterogeneous charge transfer.[21] Thus the crossover phenomenon increases when the values of the heterogeneous rate constant decrease. Further details are discussed elsewhere.[21]

If the disproportionation reaction (22) is not taken into account in the simulation, the calculated cyclic voltammograms differ markedly from the experimental results (Figure 15c). This again gives strong evidence for the validity of the ECE/EEC disproportionation mechanism. In principle, the experimental voltammograms could also be fitted with the aid of an E_iE_r disproportionation mechanism in which the chemical step is concurrent with a slow electron transfer.[40,41] However, the unambiguous experimental findings that prove the phosphine elimination rule out this alternative model.

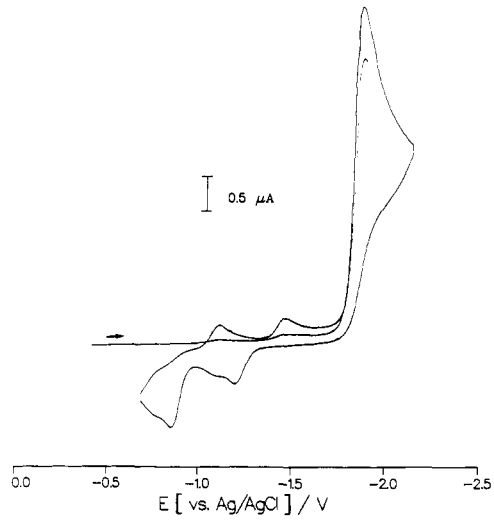

Figure 16. Cyclic voltammogram of 1.3×10^{-3} M **31** in the presence of excess CO (saturated solution). Scan rate: 0.3 V s^{-1}, $T = 24$ °C.

(c) Voltammetry of μ_3-$MeCCo_3(CO)_6(PMe_3)_3$ (31) in the Presence of Excess CO. After the cyclic voltammetry of the trisphosphine-substituted cluster had shown that during a reduction/reoxidation cycle only phosphine is liberated and readded—re-forming the starting material—further experiments in the presence of CO produced surprises. Whereas in the cathodic scan no changes were observed, independent of CO concentration, in the reverse scan at high CO concentration the original waves for the reoxidation of $[\mathbf{B}]^{2-}$ totally disappeared and several new signals emerged at potentials positively to $E^\circ_{[\mathbf{B}]^{2-}/[\mathbf{B}]^{\bullet-}}$.

These reproducible findings prove that the reaction path of trisphosphine-substituted clusters is not influenced by the presence of CO during reduction but is considerably affected by it during reoxidation. Typical results obtained with **31** are shown in Figure 16.

The waves at $E^1_{pa} = -1.54$ V and $E^2_{pa} = -0.94$ V, which indicate the reoxidation of the cathodically formed ligand deficient dianion $[\mathbf{21a}]^{2-}$ to its neutral form **21a** (see Table I above), have totally disappeared. As new signals one observes two groups of waves of different height. The first group in the anodic scan with two peaks at −1.10 and −0.97 V can be unambiguously ascribed to the oxidation of $[\mathbf{11a}]^{2-}$ and $[\mathbf{11}]^-$, while the second group, whose current is significantly higher than that of the first, has peaks at $E_{pa} = -0.81$ V and $E_{pa} = -0.71$ V. They are identified as oxidation steps for the CO-deficient dianion $[\mathbf{1a}]^{2-}$ and the anion $[\mathbf{1}]^-$ of

(42) (a) Hawley, M. D.; Feldberg, S. W. *J. Phys. Chem.* **1966**, *70*, 3459–3463. (b) Amatore, C.; Gareil, M.; Saveant, J. M. *J. Electroanal. Chem.* **1983**, *147*, 1–38.
(43) Nicholson, R. S. *Anal. Chem.* **1965**, *37*, 1351–1355.
(44) Nicholson, R. S.; Shain, I. *Anal. Chem.* **1964**, *36*, 706–723.

Scheme V

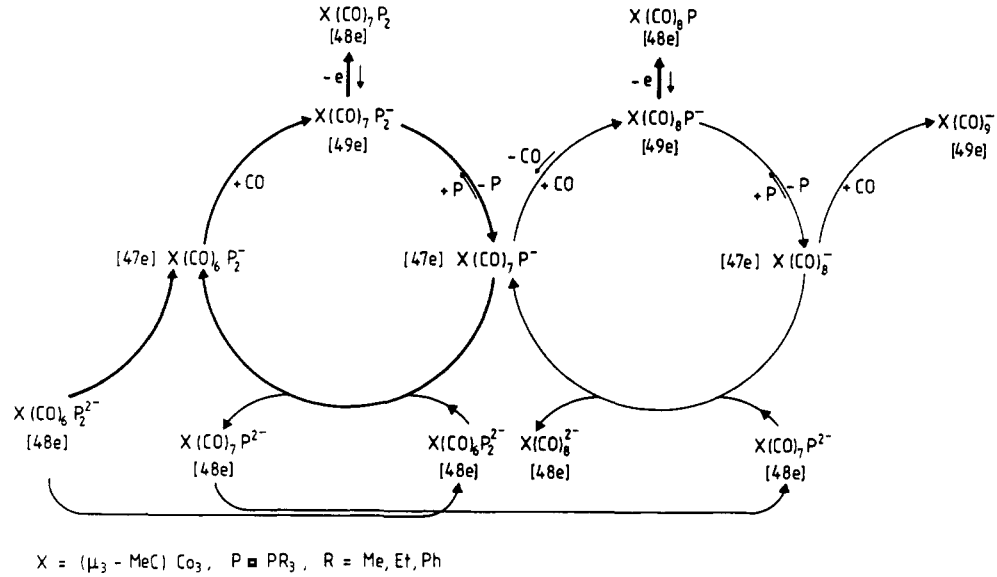

the pure carbonyl cluster. In a second cathodic scan small waves for the reduction of the newly formed species **11** at $E_{pc} = -1.12$ V and **21** at $E_{pc} = -1.46$ V can be clearly detected (see Table I). Obviously, in the presence of excess CO all trisphosphine-substituted cluster molecules involved in one cyclic voltammetric scan lose up to three phosphine ligands, which are substituted by CO. The main products generated during this process are the dianions $[\mathbf{11a}]^{2-}$ and $[\mathbf{1a}]^{2-}$.

The situation changes when the CO concentration is lowered. Figure 17 shows a series of cyclic voltammograms successively recorded at decreasing CO concentrations. Starting from a solution saturated in CO, the waves for the oxidation of $[\mathbf{1a}]^{2-}$ and $[\mathbf{1}]^{-}$ gradually decrease, while the wave for the oxidation of $[\mathbf{11a}]^{2-}$ increases. There are still no waves for the oxidation of $[\mathbf{21a}]^{2-}$ and $[\mathbf{21a}]^{-}$ (Figure 17a). Beyond a maximum current height the signal for the $[\mathbf{11a}]^{2-}$ oxidation also slowly gives way to the two typical oxidation waves of the parent cluster **31** (Figure 17b). Isopotential points are again observed. They impressively document the absence of further side reactions. Similar substitution effects are also found when bisphosphine-substituted clusters are reduced and reoxidized in the presence of excess CO.

At a first glance it seems unusual that in the presence of excess CO the stable dianion $[\mathbf{21a}]^{2-} = [\mathbf{B}]^{2-}$ generated almost exclusively during the forward cathodic scan cannot be voltammetrically observed during the reverse anodic scan. The riddle is solved by comparing the oxidation potentials of the newly formed redox couples $[\mathbf{1a}]^{2-}/[\mathbf{1a}]^{-}$ and $[\mathbf{11a}]^{2-}/[\mathbf{11a}]^{-}$ with that of the originally formed couple $[\mathbf{21a}]^{2-}/[\mathbf{21a}]^{-}$. The following relation holds: $E^{\circ}_{[\mathbf{1a}]^{2-}/[\mathbf{1a}]^{\bullet-}} > E^{\circ}_{[\mathbf{11a}]^{2-}/[\mathbf{11a}]^{\bullet-}} > E^{\circ}_{[\mathbf{21a}]^{2-}/[\mathbf{21a}]^{\bullet-}}$. This proves that the formation of $[\mathbf{11a}]^{2-}$ and even more so of $[\mathbf{1a}]^{2-}$ is thermodynamically favorable and most likely driven by an efficient ETC substitution process, in which the "starting" material, the dianion $[\mathbf{21a}]^{2-}$, is homogeneously oxidized by its follow-up products $[\mathbf{11a}]^{-}$ or $[\mathbf{1a}]^{-}$. However, by contrast to a normal ETC reaction, in which the start of the chain process is triggered, e.g., by a heterogeneous charge transfer at the electrode, causing a diminished wave of the educt in the voltammetric experiment, in this "inverse" ETC process the "starting" species, here $[\mathbf{21a}]^{2-}$, is already pushed into the catalytic cycle prior to a heterogeneous oxidation by the homogeneous disproportionation reaction (eq 22). Therefore, under an excess of CO in the reverse scan the signal for the reoxidation of $[\mathbf{21a}]^{2-}$ totally disappears. The simple reduction of the trisphosphine-substituted cluster suffices to produce ligand-deficient, CO-rich follow-up products.

The discussed reaction pattern is made more complex by the fact that the transformation of $[\mathbf{21a}]^{2-}$ first to $[\mathbf{11a}]^{2-}$ and then to $[\mathbf{1a}]^{2-}$ is based on two successive ETC cycles (Scheme V), each

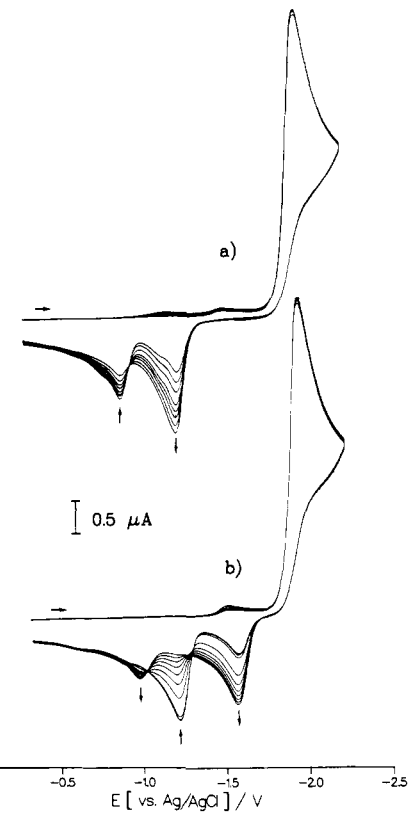

Figure 17. Cyclic voltammograms of 1.3×10^{-3} M **31** in CH_3CN/0.1 M $TBAPF_6$. Scan rate: 0.3 V s^{-1}, $T = 24$ °C. (a) Solution saturated with CO, decreasing concentration of CO in successive cycles; (b) further decreasing CO content (vertical arrows indicate the change of the current height as function of decreasing CO content).

of which involves two chemical steps, a second-order addition of CO and a first-order elimination of phosphine, each generating intermediates (eq 24 and 25).

$$[MeCCo_3(CO)_{9-n}L_{n-1}]^{\bullet-} + CO \rightleftarrows [MeCCo_3(CO)_{10-n}L_{n-1}]^{\bullet-} \quad (24)$$

$$[MeCCo_3(CO)_{10-n}L_{n-1}]^{\bullet-} \rightleftarrows [MeCCo_3(CO)_{10-n}L_{n-2}]^{\bullet-} + L \quad (25)$$

The efficiency of both cycles depends strongly on the amount of CO present in the solution. As CO adds in a second-order

reaction to the 47e intermediates, high rates are achieved only when its concentration is high. On the other hand, the rates decrease on going from phosphine-rich to phosphine-deficient species. Thus, in the case of a high excess of CO the species $[\mathbf{21a}]^{2-}$ generated via an ECE mechanism near the electrode surface is totally converted by ETC catalysis (first cycle in Scheme V) to $[\mathbf{11a}]^{2-}$. The oxidation of $[\mathbf{11a}]^{2-}$ in the reverse scan of the voltammetric experiment at $E_{pa} = -1.10$ V then triggers the second cycle, in which the main portion of $[\mathbf{11a}]^{2-}$ reacts homogeneously to $[\mathbf{1a}]^{2-}$. As intermediates and additional products of this reaction path, $[\mathbf{11}]^-$ and $[\mathbf{1}]^-$ as well as **21**, **11**, and **1** are formed either by fast addition of CO to $[\mathbf{11a}]^-$ and $[\mathbf{1a}]^-$ near the electrode surface or in a competing process by re-addition of liberated phosphine to $[\mathbf{1a}]^-$ and $[\mathbf{11a}]^-$ (Figures 16 and 17a).

By lowering the CO concentration, the second ETC cycle rapidly loses its importance. The rate-determining reaction 24 (here $[\mathbf{11a}]^- + CO$) slows down, which stops the catalytic chain process. Consequently, the wave for the oxidation of $[\mathbf{11a}]^{2-}$ increases, while the signals of $[\mathbf{1a}]^{2-}$ and $[\mathbf{1}]^-$ gradually disappear (Figure 17a). As the rate constant for the addition of CO to $[\mathbf{21a}]^-$ (eq 24) is extraordinary high, the first ETC cycle is initially not affected until the CO concentration drops to medium level.

Finally, at very low CO concentrations the initial ETC cycle will also be interrupted because the second-order CO addition to the 47e intermediate $[\mathbf{B}]^-$ ($\equiv[\mathbf{21a}]^-$) becomes so slow that the chemically resulting species $[\mathbf{11a}]^-$ can escape from the diffusion layer prior to a homogeneous redox reaction with $[\mathbf{B}]^{2-}$ (Figure 17b).

In principle, the addition of CO to $[\mathbf{B}]^-$ may already occur during the reduction of **A** (≡**31**) at the electrode, thus competing with the ECE mechanism and the above-mentioned ETC cycles. However, in this case the electron balance in the cathodic scan would remain unchanged only if the addition of CO to $[\mathbf{B}]^-$ and the subsequent elimination of the second phosphine ligand are fast under all conditions. On account of the second-order kinetics (eq 24), this is obviously not the case, which makes this mechanistic pathway very improbable.

Summary and Conclusions

The discussion has now reached a level at which it is possible to make some general statements on the reduction behavior of the tricobalt nonacarbonyl cluster **1** and its phosphine-substituted derivatives μ_3-$MeCCo_3(CO)_{9-n}(PR_3)_n$.

Starting with **1** the experimental results unequivocally prove that $[\mathbf{1}]^-$, contrary to widespread opinion, is kinetically labile and eliminates CO in a reversible reaction. As the re-addition of CO to the 47e intermediate $[\mathbf{1a}]^-$ obeys second-order kinetics, the reaction reaches thermodynamic equilibrium already at moderately high concentrations of **1** and therefore cannot be detected in the voltammetric experiment under these conditions.

In the phosphine-substituted clusters CO elimination becomes more difficult, while the rate of its (re-)addition to the 47e intermediates increases. In addition, PR_3 elimination competes with CO elimination (Scheme VI). It becomes easier with an increasing number of phosphine ligands, and for the same degree of substitution in the order $PMe_3 < PMe_2Ph < PMePh_2 < PPh_3$. As analyzed before, this dependency is mainly influenced by steric rather than electronic factors. The resulting 47e intermediates may react via different paths depending on the ligand that has been eliminated (CO or PR_3). Apart from the fact that in every case the liberated ligand may be re-added, the CO deficient species undergo phosphine addition in the presence of PR_3, thus keeping the ETC substitution process going, and in the case of the phosphine-deficient 47e intermediates either further reduction leads to stable 48e dianions or addition of CO produces CO-rich follow-up products.

The efficiencies of the different reaction paths strongly depend on the types of the phosphine ligands and on the degree of substitution. Thus, in the monophosphine-substituted clusters the anion of the PMe_3 derivative ($[\mathbf{11}]^-$) eliminates CO and PMe_3 at similar rates, hereby generating the ETC substitution product **21**, the pure carbonyl cluster $[\mathbf{1}]^-$, and the 48e dianion $[\mathbf{1a}]^{2-}$, while

Scheme VI

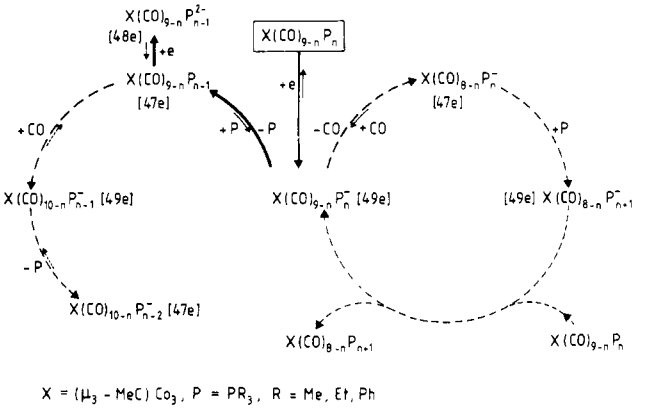

the reduction of the PPh_3 derivative produces mainly the stable 48e dianion $[\mathbf{1a}]^{2-}$. This different reaction behavior of monophosphine-substituted clusters explains why coulometric measurements of the apparent electron-transfer numbers in the series yield values between less than one and up to two. It should be mentioned here that the generation of all reduction products such as $[Co(CO)_4]^-$ or $[Co(CO)_x(PR_3)_y]^-$ that may result from cluster fragmentation during a large-scale electrolysis was not studied in this paper. Nevertheless, with the exception of $[Co(CO)_4]^-$, none of these products were observed in the measurements, indicating that under superdry conditions the fragmentation path is of minor importance.

For the bis- and trisphosphine-substituted clusters the CO elimination becomes less important. Consequently, the dianion formation dominates, and the stability of the ligand-deficient $[\mu_3\text{-}MeCCo_3(CO)_{9-n}(PR_3)_{n-1}]^{2-/1-}$ (=47e/48e) redox couples is increased. It reaches a maximum for the trisphosphine-substituted clusters where after repeated reduction/oxidation cycles only this redox couple remains in solution. Thus, the existence and stability of the 47e key intermediates in the ETC-catalyzed ligand-substitution process, which in the past were only disclosed by indirect kinetic arguments, are proven by experimental observation.

Except for this special situation, in all redox cycles described here the 47- and 49-electron species are short lived, their chemical fate being conversion to the 48e dianions or an ETC sequence leading to $[\mathbf{1}]^-$ as the most stable paramagnetic species. This is in accordance with the investigations of Robinson et al.[16a,45] and ourselves[18] on the ESR spectroscopy of anions of PR_3-substituted CCo_3 and $SFeCo_2$ clusters and of trinuclear mixed-metal clusters of the general type EM_3 with cyclopentadienyl ligands. In these extended investigations no species other than $[RCCo_3(CO)_9]^{\bullet-}$, if any, could be detected in the ESR spectra of reduced solutions, even upon electrolysis in the ESR cell and even at low temperatures and in frozen solutions. Our observation that the odd electron species do not persist in solution now makes this understandable.

The analysis of the voltammetric curves of the trisphosphine-substituted clusters has also revealed a new variant of the ECE/EEC disproportionation mechanism that involves elimination and re-addition of a ligand during the chemical steps. During the voltammetric scans homogeneous disproportionation reactions occur, leading to the observed crossover phenomenon. The experimental findings are supported by digital simulations that are in agreement with all details of the cyclic voltammetric response.

A new situation develops when an excess of CO is present. Given this prerequisite, the ligand-deficient 48e dianions of the mono- and bisphosphine-substituted clusters generated by cathodic reduction of the bis- and tris-substituted species react in very efficient ETC substitution processes to form the corresponding CO-rich dianions. In the case of the trisphosphine derivatives even two successive ETC cycles can be observed. To our knowledge these are the first examples of this "inverse" ETC process, in which

(45) Bond, A. M.; Dawson, P. A.; Peake, B. M.; Rieger, P. H.; Robinson, B. H.; Simpson, J. *Inorg. Chem.* **1979**, *18*, 1413–1417.

prior to the catalytic cycle the reacting species have been electrolytically generated.

In conclusion all the results obtained in this study may serve as a valuable basis for the interpretation of similar effects observed in other organometallic systems.

Acknowledgment. Financial support by the Baden-Württemberg Research Program (Radicals and One-Electron Transfers, FR-NW 31) and by the Fonds der Chemischen Ind. is gratefully acknowledged. J.S.F. is thankful for a Humboldt fellowship. We are indebted to F. Mallendorf for his assistance in electrochemical measurements.

Supplementary Material Available: Tables giving the experimental details of the synthesis reactions, the elemental analyses of the new compounds, and the NMR and IR data of the new compounds (4 pages). Ordering information is given on any current masthead page.

Electrochemistry and Electrocatalysis with Vitamin B_{12} in an AOT Water-in-Oil Microemulsion[1a]

Azita Owlia,[1b] Zhenghao Wang,[1c] and James F. Rusling*

Contribution from the Department of Chemistry (U-60), University of Connecticut, Storrs, Connecticut 06269-3060. *Received January 10, 1989*

Abstract: Vitamin B_{12a} solubilized in water pools of highly resistive water-in-oil (w/o) microemulsions of 0.2 M Aerosol OT (AOT, bis(2-ethylhexyl) sulfosuccinate)/4 M water/isooctane gave separate reductions of base-on cob(III)alamine to base-on cob(II)alamine ($E_{1/2}$ = −0.03 V vs SCE) and base-on cob(II)alamine to base-off cob(I)alamine ($E_{1/2}$ = −0.87 V). Diffusion coefficients suggested that vitamin B_{12} induces the formation of surfactant aggregates in w/o microemulsions that are larger than in solute-free systems. Relative reactivities toward reductions of three oil-soluble alkyl vicinal dihalides by electrochemically generated cob(I)alamine were modified in the microemulsion compared to isotropic water–acetonitrile. Changes in relative reactivity are not explained by simple partition of vicinal dibromides between isooctane and water and suggest specific interactions with surfactant aggregates or significant reaction in the bulk isooctane phase.

Clear, stable, water-in-oil (w/o) microemulsions[2] containing dynamic surfactant aggregates similar to inverted micelles can be prepared from hydrocarbon, water, and Aerosol OT [AOT, bis(2-ethylhexyl) sulfosuccinate].[3-5] Water is contained in the center of these aggregates. The anionic head groups face the "water pools", and the two hydrocarbon tails of AOT extend into the bulk hydrocarbon. Water in AOT w/o microemulsions with w_0 = [water]/[surfactant] < 10 is different from bulk water because it binds to head groups of the surfactant.[3,4] As w_0 increases, aggregate size increases and a smaller fraction of water is bound.[6]

In designing chemical systems for specific tasks, microemulsions offer the possibility of selecting reactant microenvironments as a means to control kinetics and reactivity.[4] Several reported kinetic effects of w/o microemulsions are quite dramatic. For example, the rate of aquation of tris(oxalato)chromium ion was 5×10^6 times faster in water pools of octadecyltrimethylammonium tetradecanoate than in bulk water. Rate enhancement could not be attributed simply to preconcentration of reactants in water pools.[7] Hydrolysis of *p*-nitrophenyl acetate catalyzed by imidazole decreased 50-fold in rate in AOT microemulsions because of unfavorable partitioning of reactants, i.e., catalyst resides predominantly in the water pools while *p*-nitrophenyl acetate favors the oil phase.[8a] The rate of thermocoloration of a water-soluble spiropyran was retarded 20-fold in AOT/hexane/0.6 M water. This was attributed to restricted mobility of the reactant in the water pool.[8b] Rates of axial ligand exchange of vitamin B_{12a} were enhanced up to 60 000-fold in water pools of dodecylammonium propionate or AOT in benzene.[9] Rate enhancements were amplified as w_0 decreased below 20.

The last example above is related to a specific concern of this paper, i.e., electrocatalysis with vitamin B_{12}, a naturally occurring cobalt corrin. In weakly acidic solutions, vitamin B_{12r} (cob(II)alamine) undergoes moderately fast reduction at carbon electrodes to its Co(I) form, vitamin B_{12s} or cob(I)alamine.[10,11] If an alkyl monohalide is present, it reacts with cob(I)alamine at the electrode to yield an alkylcob(III)alamine stable at the formal potential of the Co(II)/Co(I) redox couple.[11,12] However, if the alkyl halide has an appropriate activating group in the β position, the intermediate alkylcobalt complex is short lived and spontaneously decomposes to products. An example is the electrocatalytic reduction of alkyl vicinal dibromides by vitamin B_{12}, for which the pathway shown in Scheme I was proposed.[13] In Scheme I, cob(I)alamine formed at the electrode (eq 1) reacts rapidly with the vicinal dibromide RBr_2 (eq 2) to recycle cob(II)alamine at the

Scheme I

$$\mathrm{Co(II)} + \mathrm{e} = \mathrm{Co(I)} \quad (k^\circ, \text{ at electrode}) \tag{1}$$

$$\mathrm{Co(I)} + \mathrm{RBr_2} \xrightarrow{k_1} [\mathrm{BrCo(III)RBr}] \xrightarrow{\text{fast}} \mathrm{Co(II)} + \mathrm{RBr^\bullet} + \mathrm{Br^-} \tag{2}$$

$$\mathrm{Co(I)} + \mathrm{RBr^\bullet} \rightarrow \mathrm{Co(II)} + \mathrm{RBr^-} \quad \text{fast} \tag{3}$$

$$\mathrm{RBr^\bullet} \rightarrow \text{alkene} + \mathrm{Br^-} \quad \text{fast} \tag{4}$$

(1) (a) Part 7 of the series "Electrocatalysis in Organized Assemblies". (b) Present address: Mobay Corp., Baytown, TX. (c) On leave from Beijing Normal University, Beijing, China.

(2) The term microemulsion is used here for clear three-component systems of oil, water, and surfactant in which w_0 = [water]/[surfactant] > 1.

(3) Luisi, P. L.; Magid, L. *CRC Crit. Rev. Biochem.* **1987**, *20*, 409-474.

(4) (a) Fendler, J. H. *Membrane Mimetic Chemistry*; Wiley: New York, 1982. (b) O'Connor, C. J.; Lomas, T. D.; Ramage, R. E. *Adv. Colloid Interface Sci.* **1984**, *20*, 21-97.

(5) Fendler, J. H. *Acc. Chem. Res.* **1976**, *9*, 153-161.

(6) (a) Raman spectroscopy indicated[6b] about 5% of the water bound to AOT head groups at w_0 = 20. (b) D'Aprano, A.; Lizzio, A.; Liveri, V. T.; Aliotta, F.; Vasi, C.; Migliardo, P. *J. Phys. Chem.* **1988**, *92*, 4436-4439.

(7) O'Connor, C. J.; Fendler, E. J.; Fendler, J. H. *J. Am. Chem. Soc.* **1973**, *95*, 600-602.

(8) (a) Menger, F. M.; Donohue, J. A.; Williams, R. F. *J. Am. Chem. Soc.* **1973**, *95*, 286-288. (b) Sunamoto, J.; Iwamoto, K.; Akutagawa, M.; Nagase, M.; Kondo, H. *J. Am. Chem. Soc.* **1982**, *104*, 4904-4907.

(9) Fendler, J. H.; Nome, F.; Van Woert, H. C. *J. Am. Chem. Soc.* **1974**, *96*, 6745-6753.

(10) B_{12}; Dolphin, D., Ed.; Wiley: New York, 1982; Vol. I.

(11) Scheffold, R. In Scheffold, R., *Modern Synthetic Methods*; Ed.; Wiley: New York: 1983; Vol. 3, pp 355-439.

(12) Lexa, D.; Saveant, J. M.; Soufflet, J. P. *J. Electroanal. Chem.* **1979**, *100*, 159-172.

0002-7863/89/1511-5091$01.50/0